

An ~~comprehensive~~ assessment of ~~electrochemical~~ ocean alkalinity enhancement ~~in seawater using aqueous hydroxides~~: kinetics, efficiency, and precipitation thresholds

Mallory C. Ringham¹, Nathan Hirtle¹, Cody Shaw¹, Xi Lu¹, Julian Herndon^{2,3}, Brendan R. Carter^{2,3}, Matthew D. Eisaman^{4,5}

¹ Stony Brook University, Stony Brook, NY, USA

² Cooperative Institute for Climate Ocean and Ecosystem Studies, University of Washington, Seattle, USA

³ Pacific Marine Environmental Laboratory, National Oceanic and Atmospheric Administration, Seattle, WA, USA*

⁴ Department of Earth & Planetary Sciences, Yale University, New Haven, CT, USA

⁵ Yale Center for Natural Carbon Capture, Yale University, New Haven, CT, USA

* ~~Coauthors with this affiliation are included provisionally pending institutional manuscript policy review~~

Correspondence to: Mallory Ringham (mallory.ringham@stonybrook.edu); Current address: Ebb Carbon Inc., San Carlos, CA, USA

Abstract

Ocean alkalinity enhancement (OAE) is an ~~promising~~ approach to marine carbon dioxide removal (mCDR) that leverages the large surface area and carbon storage capacity of the oceans to sequester atmospheric CO₂ as dissolved bicarbonate (HCO₃⁻). ~~One OAE method involves the production of an acid (HCl) and a base (NaOH) from seawater, the return of the base to the ocean, and the removal or neutralization of the acid. involves the conversion of salt in seawater into aqueous alkalinity (NaOH), which is returned to the ocean. The SEA MATE (Safe Elevation of Alkalinity for the Mitigation of Acidification Through Electrochemistry) process uses electrochemistry to convert some of the salt (NaCl) in seawater or brine into aqueous acid (HCl), which is removed from the system, and base (NaOH), which is returned to the ocean with the remaining seawater.~~ The resulting increase in seawater pH and alkalinity causes a shift in dissolved inorganic carbon (DIC) speciation toward carbonate and a decrease in the surface-ocean pCO₂. The shift in the pCO₂ results in enhanced ~~net uptake of atmospheric CO₂ uptake or reduced CO₂ loss~~ by the seawater due to gas exchange. ~~The net result of this process is the increase of surface ocean DIC, where it is durably stored as mostly bicarbonate and some carbonate.~~ In this study, we systematically test the efficiency of CO₂ uptake in seawater treated with NaOH at ~~beaker (1L),~~ aquaria (15L), and tank (6000L) scales to establish operational boundaries for safety and efficiency in ~~advance of mesocosm studies and~~ scaling up to field experiments. ~~Preliminary results show~~ CO₂ equilibration occurred on order of weeks to months, depending on circulation, air forcing, and air bubbling conditions within the test tanks. An increase of ~0.7-0.9 mol DIC/ mol added alkalinity (in the form of NaOH) was observed through analysis of seawater bottle samples and pH sensor data, consistent with the value expected given the values of the carbonate system equilibrium calculations for the range of salinities and temperatures tested. Mineral precipitation occurred when the bulk seawater pH_T (~~total scale pH~~) exceeded 10-~~0~~ and Ω_{aragonite} exceeded 30-~~0~~. This precipitation was dominated by Mg(OH)₂ over hours to 1 day before shifting to CaCO_{3, aragonite} precipitation. These data, combined with models of the dilution and advection of alkaline plumes, will allow for estimation of the amount of carbon dioxide removal expected from OAE pilot studies. Future experiments should better approximate field conditions including sediment interactions, biological activity, ocean circulation, air-sea gas exchange rates, and mixing-zone dynamics.

Keywords

43 Ocean Alkalinity Enhancement (OAE); marine carbon dioxide removal (mCDR); ocean carbon dioxide removal
44 (ocean CDR)

45

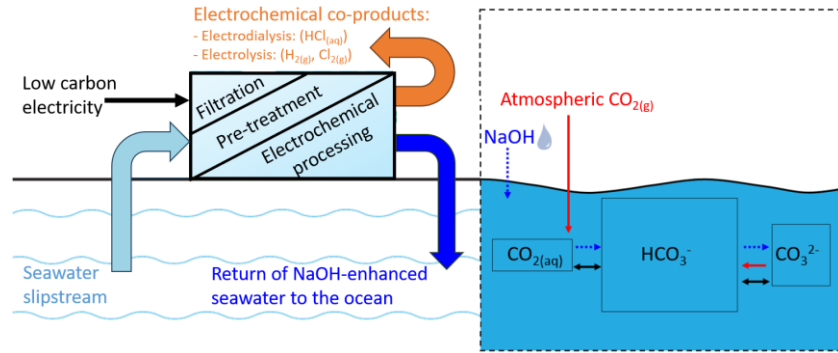
46 1 Introduction

47 The Sixth Assessment Report of the Intergovernmental Panel on Climate Change reported that in addition to a
48 drastic decrease in CO₂ emissions, active removal of ~~5-155.5~~ Gt of atmospheric CO₂ per year by 2100 is necessary
49 to constrain average global warming to less than 1.5 - 2 °C ([noting that the magnitude of carbon removals varies by](#)
50 [climate scenario](#): IPCC, 2022; Rogelj, 2018). A wide variety of negative emissions technologies (NETs) are under
51 development to meet this enormous challenge (Minx et al., 2018; NASEM, 2019; NASEM, 2021²; Rueda et al.,
52 2021; Vitillo et al., 2022).

53 A suite of promising approaches to CO₂ removal termed ocean or marine carbon dioxide removal (ocean CDR or
54 mCDR, respectively) leverage the enormous surface area and carbon storage capacity of the ocean (Boettcher et al.,
55 2019; NASEM, 2021). Ocean alkalinity enhancement (OAE) is an mCDR method that aims to store atmospheric
56 CO₂ in a dissolved phase in the ocean as bicarbonate ions (HCO₃⁻), thereby accelerating a natural planetary CO₂
57 regulation mechanism, the carbonate-silicate cycle (Berner, 1983; Isson et al., 2020). OAE has the potential to scale
58 to gigatons of CO₂ removal per year (He and Tyka, 2023), but development of this approach requires careful
59 consideration of: the methods and materials used to source and process alkalinity; the form and method of delivery
60 of alkalinity to the surface ocean (for example, aqueous or solid phase); and selection of appropriate geographic sites
61 for alkalinity dispersal (Oschlies et al., 2023). OAE methods under exploration include: mining and crushing
62 alkaline minerals (e.g., olivine, basalts) to be spread via ship or in coastal environments (e.g., beach restoration, or
63 salt marsh distribution) (Feng et al., 2017; Köhler, Hartmann, and Wolf-Gladrow, 2010; Monserrat et al., 2018;
64 Rigopoulos et al., 2018); the mining or industrial production of Mg(OH)₂ or mining CaCO₃ and calcining it to CaO
65 or Ca(OH)₂, with the Mg(OH)₂ or Ca(OH)₂ spread via ship or coastal outfall pipe (Harvey, 2008; Ilyina et al., 2013;
66 Kheshgi, 1995; La Plante, 2023; Moras et al., 2022; Nduagu, 2012; Rau, 2008; Renforth and Henderson, 2017;
67 Shaw, 2022); and the electrochemical conversion of saltwater into aqueous hydroxides and dispersal via coastal
68 outfalls (de Lannoy et al., 2018; Eisaman et al., 2018; Lu et al., 2022; Tyka, Van Arsdale, and Platt, 2022; Eisaman
69 et al., 2023; [Eisaman, 2024](#)).

70 Many of these approaches and technologies are at a nascent stage and we must move quickly to quantitatively test
71 and characterize their performance to determine which, if any, justify larger-scale deployment. The electrochemical
72 conversion of salt (NaCl) into aqueous alkalinity (NaOH) has many potential advantages in scaling considerations,
73 including simplified distribution of a liquid product to the ocean, avoidance of mining and the transportation of the
74 alkalinity source over long distances, and avoidance of potentially harmful impurities present in mined alkalinity
75 sources (NASEM, 2021; Caserini, Storni, and Grosso, 2022).

76 [Figure 1 summarizes a specific OAE approach in which electrochemical processing of seawater or brine rearranges](#)
77 [the hydrogen \(H⁺\), hydroxide \(OH⁻\), sodium \(Na⁺\), and chloride \(Cl⁻\) ions to produce acidic \(HCl\) and basic](#)
78 [\(NaOH\) solutions. From a molecular point of view, since the Na⁺ and OH⁻ ions come from the seawater itself, the](#)
79 [net result of this process is the removal of H⁺ and Cl⁻ ions from the input seawater, that is the removal of HCl acid.](#)
80 [Nothing new is added to the ocean in this process, but rather H⁺ and Cl⁻ ions are removed from seawater.](#)



81
 82 **Figure 1:** Low carbon electricity and a slipstream of seawater are the inputs to electrochemical OAE. Various
 83 process-specific filtration and pretreatment steps allow for membrane-based electrochemical processing, resulting in
 84 the removal of H^+ and Cl^- ions from seawater. The NaOH-enhanced seawater is returned to the ocean, resulting in
 85 the invasion of CO_2 into seawater and durable storage as mostly HCO_3^- and some CO_3^{2-} .

86 In the process shown in Fig. 1, a portion of the salt (NaCl) in the seawater is electrochemically separated into its
 87 constituent acid (HCl) and base (NaOH). The acid is removed, but the base is remixed with the seawater enhancing
 88 the alkalinity of the resulting seawater that is then returned to the ocean. In the case where bipolar membrane
 89 electro dialysis is used to generate the acid and base, water (H_2O) is dissociated into H^+ and OH^- ions at the junction
 90 of the bipolar membranes inside the electrochemical system (Eisaman et al. 2012). This operation alone does not
 91 change the alkalinity. But a voltage applied across a stack of ion-selective membranes then separates the H^+ and OH^-
 92 ions from each other and from the seawater, with Cl^- ions (in HCl) and Na^+ ions (in NaOH) providing the charge
 93 balance. Remixing the NaOH with the seawater but retaining the HCl results in a treated seawater solution an
 94 increased OH^- concentration $[OH^-]$ compared to the input seawater.

95 Total alkalinity (TA) is defined as the excess of proton acceptors over proton donors in an aqueous solution (Eq. 1),
 96 where ellipses represent neglected acids and bases (Dickson 1981; Dickson 1992; Wolf-Gladrow et al., 2007). A
 97 higher TA value for a seawater sample indicates that it has a higher buffering capacity than a sample with a lower
 98 TA value. That is, for sample with a higher TA value, the addition of a given amount of acid to the sample will
 99 decrease its pH less than for a sample with a lower TA value.

100
$$TA = [HCO_3^-] + 2 [CO_3^{2-}] + [B(OH)_4^-] + [OH^-] + [HPO_4^{2-}] + 2 [PO_4^{3-}] + \dots - [H^+] - [HSO_4^-] - \dots \quad (1)$$

101 Most of the OH^- from NaOH addition rapidly reacts with other molecules in seawater, but Eq. (1) is formulated so
 102 the total remains unchanged through these reactions. From Eq. (1), we see the increased-additional OH^-
 103 concentration in a treated seawater solution corresponds to a salt solution with increased alkalinity relative to the
 104 starting salt solution. The reason that the H^+ concentration remains the same even though H^+ ions were removed is
 105 that both the H^+ and OH^- started as bound in an H_2O molecule, which was then dissociated into free H^+ and OH^- ions
 106 at the bipolar membrane junction. Therefore, upon removing the H^+ ions but remixing the OH^- ions, the H^+ ion
 107 concentration is the same as prior to H_2O dissociation, while the OH^- ion concentration is increased. The OH^- reacts
 108 with and consumes free H^+ , thereby increasing this increase in OH^- ion concentration rapidly increases the
 109 seawater pH upon mixing. The OH^- also accepts protons from bicarbonate and the carbonic acid formed from the
 110 reaction with CO_2 and H_2O , resulting in a shift of the dissolved inorganic carbon (DIC) speciation towards carbonate
 111 according to the net reactions (Eisaman et al., 2023):



114 ~~this process may have the potential to locally and transiently mitigate the elevated $p\text{CO}_2$ associated with ocean~~
 115 ~~acidification (NASEM, 2021; Cross et al., 2023; Butenschön et al., 2021).~~ The concentration of dissolved CO_2 gas
 116 ($\text{CO}_{2,\text{aq}}$) in this alkalinity-enhanced seawater is less than it would be if it were in equilibrium with atmospheric CO_2
 117 (Equation 2b). Over the longer timescale required for air-sea gas exchange - weeks to months (Wang et al., 2023) or
 118 months to years (He and Tyka, 2023) depending on location - the disequilibrium in the surface ocean resulting from
 119 the alkalinity addition drives the invasion of atmospheric CO_2 into seawater (or lessens the outgassing of CO_2 from
 120 the surface ocean to the atmosphere), where it reacts with carbonate and is stored primarily in the stable bicarbonate
 121 phase (Jones et al., 2014; Bach et al., 2023; Renforth and Henderson, 2017; Eisaman et al., 2023).



124 ~~As net reaction (2b) takes significantly longer than net reaction (2a), this process may have the potential to locally~~
 125 ~~and transiently mitigate the elevated $p\text{CO}_2$ and loss of carbonate ions associated with ocean acidification (NASEM,~~
 126 ~~2021; Cross et al., 2023; Butenschön et al., 2021) even though most of the carbonate ion that is initially produced (in~~
 127 ~~Eq. 2a) is eventually consumed (in Eq. 3b). Also, a fraction of the carbonate is not consumed, and even~~
 128 ~~once equilibrium has been reached, the net reaction can be written as equation 4 (Eisaman et al., 2023):~~



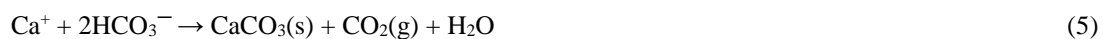
130 ~~where the coefficients a-e depend on seawater properties such as temperature, pressure, and pH through the~~
 131 ~~dependence of the equilibrium constants on these variables. Under typical ocean conditions, after equilibrium has~~
 132 ~~been reached, OAE results in an increase in the DIC in seawater on the order of ~0.7-0.9 moles of DIC per mole of~~
 133 ~~NaOH added, depending on seawater conditions. Following equilibration after OAE, the final slightly~~
 134 ~~increased pH and carbonate ion concentrations are slightly increased relative to the initial values (He and Tyka,~~
 135 ~~2023). For common surface ocean conditions (e.g., 20°C, salinity 35, and initial TA of 2000 $\mu\text{mol kg}^{-1}$) at complete~~
 136 ~~equilibrium, calculated values of a=0.84, b=0.71, c=0.13, d=0.002, e~1 can be obtained, which would correspond to~~
 137 ~~0.84 moles of DIC per mole of NaOH.~~

138 It is possible that air-sea gas exchange will not completely drive the seawater $p\text{CO}_2$ to the initial unperturbed value
 139 before the seawater sinks into the ocean interior and loses contact with the atmosphere for hundreds to thousands of
 140 years. Therefore, the DIC anomaly relative to the alkalinity anomaly present when the seawater sinks into the ocean
 141 interior may be used to assess the effective impact of the OAE for capturing atmospheric CO_2 on the 0-100 year
 142 timescales that are most important for climate interventions.

143 ~~In addition to the storage of atmospheric CO_2 in the form of DIC, this process may have the potential to locally and~~
 144 ~~transiently mitigate the elevated $p\text{CO}_2$ associated with ocean acidification (NASEM, 2021; Cross et al., 2023;~~
 145 ~~Butenschön et al., 2021). In a water body with a finite seawater exchange rate with the ocean, such as a semi-~~
 146 ~~protected estuary or bay, alkalinity could be added in a controlled manner such that the combination of the rapid~~
 147 ~~reactions described by Eq.(1) and the exchange/flushing rate with the open ocean result in the bay being held in~~
 148 ~~steady state at a target pH or aragonite saturation state value that is higher than its equilibrium value under~~
 149 ~~conditions of ocean acidification. As this added alkalinity diffuses through the bay and makes its way to the open~~
 150 ~~ocean, CO_2 removal and storage as DIC would occur. By metering the rate of alkalinity addition to the bay to match~~
 151 ~~the flushing rate, the pH or saturation state of the bay can be held at a constant target value. Even once equilibrium~~
 152 ~~has been achieved in the open ocean, the pH and the carbonate ion concentration in the open ocean remains slightly~~
 153 ~~higher than before the alkaline discharge. However, the absolute value of this pH increase after equilibrium has been~~
 154 ~~reached is sufficiently small relative to the alkalinity and DIC increase that mitigating ocean acidification on a~~
 155 ~~global scale with this method is unfeasible. For example, increasing the equilibrium pH value from 8.0 to 8.1 at a~~
 156 ~~fixed $p\text{CO}_2$ of 400 μatm (at 20 C and 35 salinity with no macronutrients) requires a TA increase of around 620~~

157 ~~μmol/kg sw and a DIC increase of around 520 μmol/kg sw. Using these numbers, mitigating OA over the entire 360~~
158 ~~million km² surface of the ocean to a depth of 100 meters would require around 487 gigatons of cumulative CO₂~~
159 ~~removal. In addition to the storage of atmospheric CO₂ in the form of DIC, this process may have the potential to~~
160 ~~locally mitigate ocean acidification. In a water body with a finite seawater exchange rate with the ocean, such as a~~
161 ~~semi-protected estuary or bay, alkalinity could be added in a controlled manner such that the combination of the~~
162 ~~rapid reactions described by Eq.(1) and the exchange/flushing rate with the open ocean result in the bay being held~~
163 ~~in steady state at a target pH or aragonite saturation state value that is higher than its equilibrium value under~~
164 ~~conditions of ocean acidification. As this added alkalinity diffuses through the bay and makes its way to the open~~
165 ~~ocean, CO₂ removal and storage as DIC would occur. Even once equilibrium has been achieved, the pH and the~~
166 ~~carbonate ion concentration in the open ocean remains slightly higher than before the alkaline discharge. By~~
167 ~~metering the rate of alkalinity addition to the bay to match the flushing rate, the pH or saturation state of the bay can~~
168 ~~be held at a constant target value. We refer to this approach as the SEA MATE process: the Safe Elevation of~~
169 ~~Alkalinity for the Mitigation of Acidification Through Electrochemistry.~~

170 Deploying ~~SEA MATE~~this OAE process in the ocean or coastal waters will require an understanding of carbonate
171 chemistry in seawater in the ocean volume under consideration, as well as thresholds for safe operation. For
172 example, at the point of alkaline dispersal where there is the maximum change in seawater chemistry, ~~SEA MATE~~
173 ~~must control the~~the rate of alkalinity addition must be controlled relative to the rate of mixing and dilution in the
174 ocean to avoid the precipitation of Mg(OH)₂ or CaCO₃ (Hartmann et al., 2023; Moras et al., 2022). While Mg(OH)₂
175 readily redissolves, an increase in turbidity due to precipitation may negatively affect marine organisms (Bainbridge
176 et al., 2018; Broderson et al., 2017; ~~Dutertre et al., 2009~~). By contrast, CaCO₃ will generally not redissolve in the
177 surface ocean without biological mediation, and runaway precipitation, where alkalinity removed by precipitation
178 exceeds that added by the OAE treatment, can occur under conditions of increased aragonite saturation state and in
179 the presence of increased mineral nucleation sites in the water column (Moras et al., 2022). CaCO₃ precipitation
180 could counteract the intended effect of the OAE intervention by removing alkalinity from the surface ocean and
181 releasing CO₂ gas via Eq. 5 (Zeebe and Wolf-Gladrow, 2001):



183 Upon dispersal to the ocean through a coastal outfall pipe, the added alkalinity is advected and ~~diffuses mixed~~
184 from the point source, becoming increasingly diluted ~~through the mixing zone over time~~. Because the timescale for
185 air-sea gas exchange and re-equilibration described by Eq. (2) is longer than the characteristic timescale for dilution
186 driven by tides, currents, and weather, most of the CO₂ removal occurs far from the mixing zone. Dilution will
187 spread the impacts over a sufficiently broad area, ~~to an extent~~ that it is unlikely that the impacts on the DIC
188 distribution can be quantified using only direct measurements; given current instrument resolution and the typical
189 dynamic range of natural variability (Wang et al., 2023). In general, options for measurement, reporting, and
190 verification (MRV) of OAE will therefore rely on (Ho et al., 2023): experimentation in laboratory and mesocosm
191 settings, such as the work we describe here, to establish CO₂ removal dynamics under conditions of OAE; direct
192 monitoring of the rate and characteristics of alkalinity addition into seawater; monitoring the seawater carbonate and
193 environmental chemistry in the immediate vicinity of the outfall via sensors and sampling (Cyronak et al., 2023;
194 Schulz et al., 2023); and ocean modeling to estimate CDR beyond the range of direct detection (Fennel et al., 2023).

195 While some work has investigated various aspects of NaOH-based ocean alkalinity enhancement in microcosms
196 (Ferderer et al., 2022; Hartmann et al., 2023), ~~and in~~ mesocosms (Groen et al., 2023), and other work has studied the
197 release of NaOH over natural coral reefs as a method of local ocean acidification mitigation (Albright et al., 2016), a
198 systematic characterization of the efficiency and kinetics of OAE as a function of key process parameters has not yet
199 been performed. Here we report the first tank-scale tests of OAE that use aqueous hydroxide (NaOH) to enhance the
200 alkalinity of natural seawater, a process that mimics OAE via ~~the~~ electrochemical brine-to-alkalinity conversion
201 used in the SEA MATE process. Our experiments, conducted in 6,000 liter tanks using seawater pumped from Flax

202 Pond on Long Island Sound in Stony Brook NY, quantify the magnitude and timescale of the CO₂ removal from the
203 air and storage as seawater DIC by monitoring the air-seawater re-equilibration after an initial alkalinity
204 perturbation. In addition, our use of both laboratory-processed bottle samples and field-deployable sensors to
205 measure and over-constrain the carbonate chemistry response allows us to assess the suitability of certain sensing
206 platforms for MRV. Finally, we investigate safe thresholds for the rate and concentration of alkalinity addition to
207 avoid: (1) the precipitation and redissolution of Mg(OH)₂ that can lead to local, temporary increases in turbidity; and
208 (2) the precipitation of CaCO₃, which partially reverses the intended OAE effect by removing alkalinity from, and
209 releasing CO₂ gas into, the surrounding seawater.

210 Using this approach, we address the following key questions:

211 (1) How much additional atmospheric CO₂ is stored in seawater as DIC in response to a given alkalinity
212 perturbation?

213 (2) What is the timescale for CO₂ removal from the air for these tanks, and how does it depend on the pHT following
214 OAE and the magnitude of alkalinity enhancement?

215 (3) ~~If-What are the conditions for Mg(OH)₂ precipitates-precipitation upon addition of NaOH to seawater, on what~~
216 ~~spatial and temporal scales does it redissolve??~~

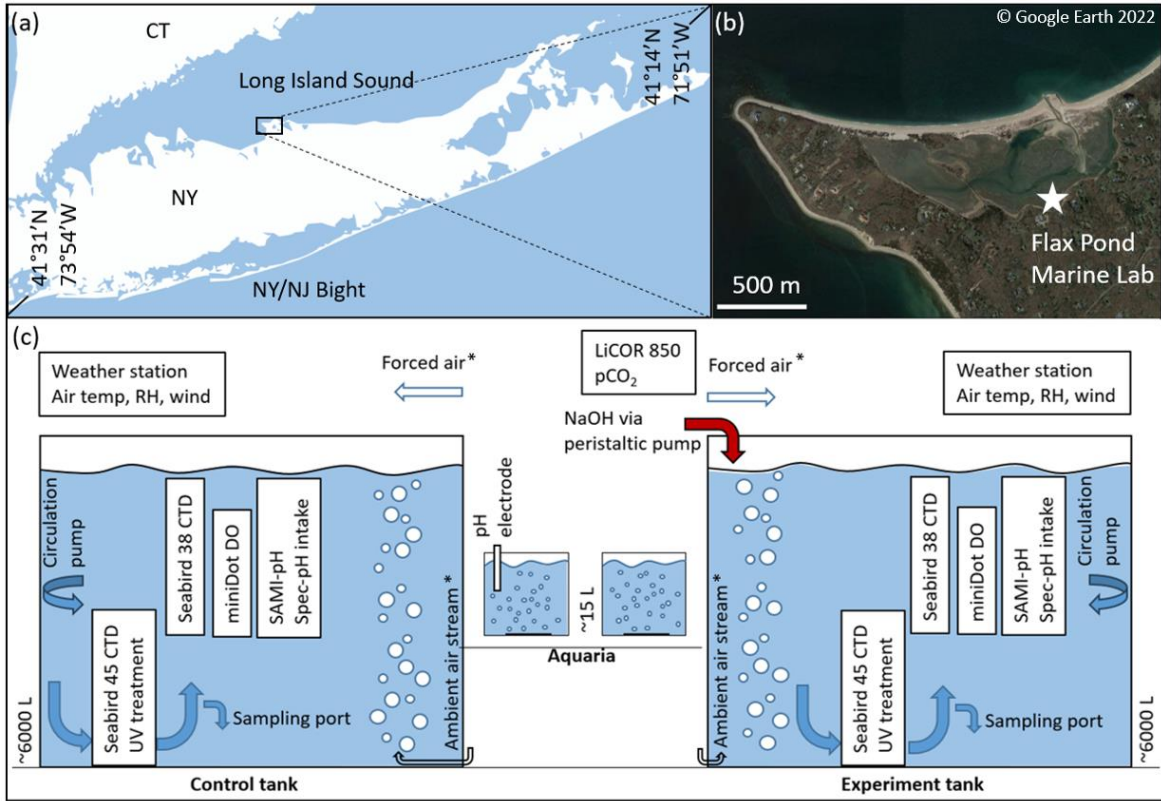
217 (4) What are the threshold values for ~~pH-pHT~~ and aragonite saturation state beyond which undesired CaCO₃
218 precipitation will occur?

219 Answering these questions is key to assessing the viability of this approach and to optimizing its eventual
220 deployment. The large tank experiments presented in this manuscript provide a stepping stone between bench-scale
221 experiments and in-situ mesocosms or field pilots, and are among the largest experiments that can be conducted with
222 a control seawater reference reservoir. Even if these experiments simply confirm stoichiometric and modeled
223 expectations, this is critical information in the design and implementation of OAE deployments. This work is a
224 necessary part of the growing scientific body that will allow for field trials to progress.

225 2. Methods

226 2.1 Experimental procedure

227 We investigated the carbonate chemistry changes resulting from the addition of NaOH_(aq) to natural seawater over
228 timescales ranging from 2 weeks to 2 months in a series of experiments at two scales: (1) two large (~6200 L)
229 indoor tanks, and (2) multiple 15 L aquaria (Fig. 12).



230

231 **Figure 12:** (a, b) Flax Pond Marine Laboratory is located on Long Island Sound, New York, USA (© Google Earth
 232 2022). (c) The ~6000 L control and experiment tanks were instrumented with a series of oceanographic sensors and
 233 sampled routinely for DIC/ TA analyses to allow for measurement of carbon uptake over time following an addition
 234 of alkalinity in the form of NaOH. The ~15 L aquaria were instrumented with standard glass pH electrodes and
 235 monitored with routine TA analyses. The Forced air* and Ambient air streams* indicate their use in some but not all
 236 experiments, as noted in later sections.

237 This study was conducted at the Flax Pond Marine Laboratory at Stony Brook University, NY. All experiments used
 238 natural seawater collected from Flax Pond, part of a 128-acre salt marsh tidal wetlands connected to the Long Island
 239 Sound. The surface areas of the tanks and aquaria were ~4.6 m² and ~0.1 m², respectively. The tanks had a diameter
 240 of 0.224 m, a total height of 1.52 m, and were typically filled to a height of ~1.35 m, allowing for a corresponding
 241 seawater volume of 6185 L. The aquaria had a diameter of 0.3 m and were typically filled to a height of ~0.23 m, for
 242 a total seawater volume of 15 L. The large tank volumes were chosen to limit interactions with walls while
 243 increasing the air-seawater boundary, and to lose a smaller fraction of their volume to evaporation. ~~and~~ These
 244 tanks allow for in-situ oceanographic sensor deployment and frequent bottle sampling while retaining semi-
 245 controlled temperature, mixing, filtration, and biological control. The inherent limitations of these tank tests include
 246 limited air-sea interaction, unrealistic light levels and circulation, and biological responses that are not a perfect
 247 representation of natural seawater in the ocean, but serve as a stepping stone to mesocosm and eventual field
 248 experiments. On average, the large (~6,000 L) tank experiments took ~6.5 weeks after dosing with NaOH to reach
 249 90% of the calculated or extrapolated asymptotic ΔDIC/TA addition ratio indicative of full air-seawater equilibrium,
 250 as will be discussed in Section 3. Therefore, in addition to the large tank tests, we conducted a series of smaller
 251 aquaria alkalinity additions to increase our capacity for experimental test cases. The limitations of the aquaria
 252 include limited sensor options, unrealistic circulation, and limited biological control. While it is expected that
 253 equilibration occurs more rapidly in the small aquaria than in the large tanks, the results from these cases should be
 254 similar after both experiment types have been allowed to fully equilibrate as CO₂ equilibrates CO₂ across the air-

255 seawater boundary. However, we note that some variation is expected due to limited sensing and sampling options
256 in the smaller aquaria and the greater potential for biological growth in the large tanks over longer timescales.

257 2.1.1 Tank experiments

258 Seawater was pumped into the tanks at high tide through a series of sock filters to exclude macroscopic biology. The
259 tanks were then dosed to 40 ppm bleach (sodium hypochlorite) and the shock-treated seawater was allowed to
260 circulate through the tanks for ~1 day to limit biological growth. The seawater was then circulated through UV light
261 arrays to break down the bleach over ~1-2 weeks, as assessed by a standard Hach test kit for free chlorine. During
262 this period, seawater was pumped between the two large test tanks (~25 L/min) to increase mixing of the bleach and
263 to homogenize the tanks to similar initial conditions. For the remainder of each experiment, the seawater was
264 continually pumped through the UV sterilizers. Measurements of total alkalinity showed no significant differences
265 in the bulk seawater TA before and after the bleaching process in any experiment or control tank.

266 Oceanographic sensors and discrete daily bottle sampling, as described in Sections 2.2 and 2.3, respectively, were
267 deployed for carbonate chemistry analysis for several days prior to the alkalinity addition to understand the initial
268 baseline conditions in both tanks. Two submerged pumps were used for water circulation within each tank: the first
269 pump (Current eFlux DC Flow Pump, 210 GPH) cycled seawater through the UV arrays with an estimated
270 overturning time of the bulk tank on order of 1 day, and a second (Kedsum Submersible pump, 260 GPH), mounted
271 at an angle halfway down the tank wall, allowed for subsurface circulation within the tank to reduce the occurrence
272 of unmixed ‘dead zones’ and subsequent non-homogenous biological growth, as assessed visually on the surface of
273 the water and/or tank lining. Initial tank experiments were conducted with a still surface condition, i.e., with no
274 visible water movement across the surface of each tank. As experiments progressed, forced air movement was added
275 across the surface of each tank using a stationary fan with a wind speed of ~5 kph. This was done to control for
276 potential variations in the laboratory HVAC system and to potentially reduce the time to equilibration for the
277 experiments by increasing the rate of air-sea CO₂ equilibration. In later experiments, air was bubbled into the bottom
278 of each tank at a rate of ~ 30 L min⁻¹ with an estimated surface area of ~ 0.3 m², with a goal of further increasing the
279 rate of equilibration to allow for more rapid throughput of experiments. These variations are further discussed in
280 Section 2.4. With exceptions discussed in Section 2.4, the surface of each tank was still throughout the experiments.

281 After baselining, one tank (referred to as the “experimental tank”) was dosed with enough 0.5 M NaOH (see
282 Supplementary Materials) to raise the bulk seawater pH_T to the target pH_T of interest for a given experiment, and the
283 same volume of DI water was added to the other tank (referred to as the “control tank”). NaOH additions were
284 typically dosed into the tank via peristaltic pump at a low enough rate (~50 mL/min) that a steady increase in bulk
285 tank pH_T was observed, but local pH_T measured just below the NaOH introduction never exceeded a pH_T of 9.0. A
286 pump (~25 L/min) was placed just below the NaOH stream to speed the mixing of NaOH into the bulk tank,
287 increase dilution from the point source, and to prevent the immediate precipitation of Mg(OH)₂ upon contact of the
288 NaOH with seawater. This pump was removed after the full volume of NaOH was mixed into the tank.

289 After the alkalinity addition, the tanks were left to equilibrate with the atmosphere and were monitored by sensors
290 and sampling as described in Sections 2.2 and 2.3. The tanks were indoors in the wet laboratory at Flax Pond Marine
291 Lab, such that temperature and CO₂ concentration were moderated by the building’s HVAC system, but varied
292 throughout days and seasons depending on other uses of the lab space. The experiments were concluded when the
293 observed pH_T or DIC (calculated from daily pH_T and frequent TA measurements) appeared to stabilize (e.g., ΔpH_T
294 ±0.05% or ΔDIC ±10 μmol kg⁻¹ per day) over several days, though we note that early experiments were terminated
295 before full equilibration. The continuous improvement of experimental methods during this study resulted in some
296 minor variations among the methods used for each experiment, including methods of NaOH dosing, tank circulation,
297 and biological control, as discussed where necessary in Section 3 and in the Supplementary Materials.

Seawater carbonate chemistry measurements were used to analyze the uptake of CO₂ in each tank, primarily relying on calculations from the NOAA/PMEL DIC and TA analyses of bottle samples when available (described in Section 2.3) and using sensor pH_T and Stony Brook TA measurements for cross-verification or to fill in between discrete DIC samples. DIC and TA data were normalized to the salinity at the start of a given experiment to account for evaporation (Friis et al., 2003). Carbonate chemistry calculations were then performed using CO2SYS (Lewis and Wallace, 1998), with Lueker et al. (2000) carbonate constants, Dickson (1990) for KSO₄, and Lee et al. (2010) for total boron. Wherever possible, a combination of CRM analyses and comparisons between simultaneous pH_T sensor and NOAA PMEL bottle samples were used to correct SAMI-pH and spectrophotometric pH_T sensor data for drift.

Changes in the seawater carbonate chemistry over time were analyzed with respect to shifts away from the baseline within a single control or experiment tank, as well as with respect to the differences between the control and experimental tanks. Henry's law and CO2SYS calculations were used to estimate the initial and final equilibration condition of each tank experiment. LicOR pCO_{2,atm} measurements were averaged across experiments to a representative value (421 ± 14 ppm), which was used with the initial seawater temperature and salinity to estimate pCO_{2,seawater} at the beginning of each experiment. The initial equilibrium DIC was estimated from a CO2SYS calculation using the pCO_{2,seawater} and nTA_i. The final equilibrium nDIC was estimated from a CO2SYS calculation using the same pCO_{2,seawater} and the nTA measured just after the NaOH addition, corrected for the linear increase in salinity over the course of the experiment. The ratio of the expected ΔnDIC calculated at equilibrium with the atmosphere to the addition of alkalinity provides a simple estimate of the expected CO₂ storage capacity for a given experiment. The percent equilibration for each experiment was then estimated from the measured and expected values for CAR.

2.1.2 Aquaria experiments

The large volume of tank experiments allowed for precise measurement of the seawater carbonate chemistry via bottle sampling (1L each, sent to NOAA/PMEL for analysis) with high sampling frequency. To compliment these measurements, we also performed a series of experiments in smaller aquaria (15 L each), which enabled a larger number of replicates and a faster time to equilibrium when bubbled with air. A series of polycarbonate aquaria were filled with 15 L of seawater taken from the large control tank just after the described bleaching and bleach breakdown procedure was completed. NaOH was dosed into each aquaria to reach a targeted bulk pH_T, with a corresponding volume of DI H₂O added to the control aquaria, and then the seawater was allowed to equilibrate with atmospheric pCO₂ over days to weeks. The aquaria did not have either UV light arrays for biological control or aquarium pumps for internal circulation. In most cases, the aquaria were bubbled with air (~4 L_gmin⁻¹) via a standard aquarium bubbling bar spanning the center diameter of each aquarium to reduce the equilibration time of these experiments compared to the large tank experiments for all initial pH_T conditions investigated. There was no fine control on air bubbling, but the surface area of all air bubbles in a given aquarium at any point in time was estimated at ~0.01 m². No sensors were deployed in the aquaria due to their limited size, and seawater chemistry was established via discrete pH_T and TA measurements (Sect. 2.2).

As shown in Eq. (6), we define the dimensionless 'Carbon-to-Alkalinity Ratio' (CAR) for our experiments as the molar ratio of the increase in nDIC (in units of μmol/kg, normalized to the system's initial salinity to account for evaporation) to the magnitude of the TA increase (ΔTA, in units of μmol/kg). nDIC_{equi} is the measured (via direct titration) or calculated (via CO2SYS using measured TA and pH_T) DIC value that the system reached at the end of an experiment (Pierrot et al., 2006; Van Heuven et al., 2011). Some experiments were left long enough to achieve equilibration with atmospheric CO₂, but others were halted early. In these cases, a CO2SYS calculation was used to estimate the DIC increase expected at equilibration given initial seawater conditions, and the difference between this value and the final recorded nDIC_{equi} was used to estimate the overall percent equilibration for a given experiment. Depending on experimental constraints described in later sections, nDIC_i may represent either: (1) the final nDIC measured (via titration of bottle samples) or calculated (via CO2SYS using seawater TA and pH) in the control tank,

343 or (2) the ‘baseline’ $nDIC$ before the addition of NaOH to a given aquaria experiment, for cases where a
344 corresponding control case may not be available. Note that because we are reporting CAR values where the
345 measured DIC has reached or has been estimated at equilibrium, the CAR values we measure and report reflect the
346 ratio of ΔDIC to ΔTA that would be expected given sufficient time for air-sea exchange to reach equilibrium, and so
347 are equivalent to directly measuring the value of the “TA addition potential impact ratio” as defined by Wang et al.,
348 2023.

349 Carbon-to-Alkalinity Ratio (CAR) = $(nDIC_{equ} - nDIC_i) / \Delta TA$
350 —————(6)

351 Not all aquaria experiments were directly comparable to the aquaria control. Seawater for one control aquarium was
352 collected in March 2023 and was monitored for pH_T and TA changes beginning in March 2023 and concluding in
353 May 2023. Seawater for the experimental aquaria was collected in three batches between March, April, and May
354 2023, with only 4-6 aquaria experiments running in parallel within each set of experiments due to space and
355 analytical throughput constraints. Because of this, the experiments started in March 2023 could be compared directly
356 to the control (target pH_T 8.3, 8.5, 8.5 still, and 8.7), but the rest of the experiments used different initial seawater
357 than the control aquaria. The CAR for each aquaria experiment was therefore calculated from changes in DIC and
358 TA between the initial ‘baseline’ condition and after the NaOH was added within a given aquarium, rather than
359 between the experiment and control cases.

360 With the exception of a single target pH_T 8.5 experiment, all aquaria were bubbled with ambient air, allowing for
361 rapid CO_2 exchange, and an optically clear lid was placed on each aquarium to reduce evaporation and splashing
362 onto nearby equipment. Some evaporation was evident from the rising TA throughout these experiments, but was
363 not resolvable within the resolution of a handheld salinometer used for these experiments, which ranged from values
364 of 30 -- 31 during the experiments. Therefore, DIC and TA were not normalized to salinity in these cases.
365 Temperature was discretely recorded from a combination Ross pH electrode.

366 Each aquaria was gently stirred during the addition of NaOH to prevent $Mg(OH)_2$ precipitation. After the addition of
367 NaOH, the aquaria were allowed to equilibrate with atmospheric CO_2 . Similar to the large tank experiments, we
368 used Henry’s law and CO2SYS calculations to estimate the initial and final equilibration condition of each aquaria
369 experiment. The same average $pCO_{2,atm}$ of 421 ± 14 ppm was used with the initial seawater temperature and salinity
370 to estimate $pCO_{2,seawater}$ at the beginning of each experiment. The initial equilibrium DIC was estimated from a
371 CO2SYS calculation using this $pCO_{2,seawater}$ and TA_i . The final equilibrium DIC was estimated from a CO2SYS
372 calculation using the same $pCO_{2,seawater}$ and the TA measured just after the NaOH addition. The percent equilibration
373 for each experiment was then estimated between the measured and predicted values for $\Delta DIC / \Delta TA$. Due to the air
374 bubbling, most experiments approached equilibrium with the atmosphere within 1-7 days, with the exception of the
375 non-bubbled pH_T 8.5 experiment that took ~20 days. The surface water of this non-bubbled experiment was
376 stagnant, and the water was only mixed via stirring just before taking pH_T and TA samples.

377 2.2 Oceanographic sensors

378 Each tank was instrumented with a series of sensors placed halfway down the wall of the tank near the inlet of the
379 UV circulation pump. A Seabird 38 Digital Oceanographic Thermometer and Seabird 45 MicroTSG
380 Thermosalinograph continuously monitored seawater temperature and salinity, respectively. Dissolved oxygen was
381 measured by a PME miniDOT Logger at 10 min resolution. pH_T was monitored daily by a SAMI-pH (manufacturer
382 specified accuracy/precision ~ 0.003/0.001, though this accuracy is likely an underestimate of the uncertainty given
383 known challenges for the calibration of the pH_T measurements) and by a semi-automated spectrophotometric (spec-
384 pH) pH_T unit ($\sim \pm 0.0055/0.0004$) as described by Carter et al. (2013). CRM measurements were taken by each pH_T
385 system at the beginning and end of each experiment and were used alongside discrete samples of DIC and TA as

386 described in Section 2.3 to constrain the stability of each sensor. The SAMI-pH measurements were recorded at
387 ambient seawater temperature and corrected for in-situ salinity as recorded by the Seabird Thermosalinograph
388 following best practices from the manufacturer. The spec-pH_T analyses occurred in a jacketed cuvette held at 20 °C
389 (regulated via water bath) and were corrected to the in-situ bulk tank temperature and salinity as recorded by the
390 Seabird Thermometer and Thermosalinograph. Both the SAMI-pH and spec-pH_T rely on spectrophotometric
391 analysis of metacresol purple indicator dye, which allows for pH_T measurement within the pH_T range of
392 approximately 7 to 9. For experiments in which enough NaOH was dosed into seawater to raise pH_T above these
393 limits, a Thermo Scientific Orion ROSS Ultra pH/ATC Triode combination electrode (8157BNUMD) was used to
394 monitor pH_{NBS} at the surface of the tank (± 0.01 precision), which was then converted to pH_T for comparison with the
395 other pH_T [sensor-measurement](#) systems.

396 A LiCOR LI-850 sensor was used to analyze atmospheric $p\text{CO}_2$ ($\pm 1.5\%$ accuracy) above the tanks. The inlet to this
397 sensor was periodically moved between tanks to ensure that atmospheric $p\text{CO}_2$ in the vicinity of the control and
398 experiment tanks was the same. AcuRite Iris weather stations were mounted on the side of each tank to monitor air
399 temperature (± 2 °C), relative humidity ($\pm 3\%$), and air speed (± 0.8 m s⁻¹). All data were compiled on an hourly basis
400 in a custom R package.

401 2.3 Discrete sampling

402 Two types of discrete sampling were used to constrain carbonate chemistry throughout these experiments. First, 500
403 mL of seawater was collected and preserved from each tank, typically on a daily basis, and as frequently as hourly
404 during the addition of NaOH, following best practices laid out by Dickson (2007) including overflowing of the
405 sample bottles during collection and addition of 0.2 mL of saturated mercuric chloride (HgCl₂) as a preservative.
406 These bottle samples were analyzed for DIC and TA at NOAA Pacific Marine Environmental Laboratory
407 (NOAA/PMEL). DIC concentrations were measured using a coulometer (UIC Inc.) and Single Operator
408 Multiparameter Metabolic Analyzer (SOMMA) (Johnson et al., 1985; ~~1993~~). TA was determined by an open-cell
409 acidimetric titration (Dickson et al. SOP 3b, 2007). The accuracy of DIC and TA measurements was assessed with
410 Certified Reference Materials (CRMs, supplied by the Dickson laboratory at Scripps Institution of Oceanography),
411 and overall uncertainty for both DIC and TA was typically $\pm 0.1\%$ (~ 2 $\mu\text{mol/kg}$).

412 In addition, discrete seawater samples were analyzed for TA via open-cell potentiometric titration at Stony Brook
413 University. A Thermo Scientific Orion ROSS Ultra pH/ATC Triode combination electrode (8157BNUMD),
414 calibrated using three buffer solutions (pH_{NBS} 4.01, 7, and 10.01) was used to track the titration of a ~ 20 mL
415 seawater sample with a dilute HCl solution (~ 0.1 M in 0.7 M NaCl, calibrated daily with CRM or a secondary
416 seawater standard) following a modified Gran titration procedure using a KloeHN digital syringe pump (Song et al.,
417 2020; Wang and Cai, 2004). The precision of TA measurements was $\sim \pm 5$ -10 $\mu\text{mol/kg}$. This TA data was corrected
418 to that of the bottle samples analyzed via titration at NOAA PMEL where available (see Supplementary Materials).

419 There are several differences between the aquaria experiments and the larger tank experiments. First, the aquaria
420 experiments were monitored daily to every few days by discrete measurement of TA at Stony Brook University and
421 pH_{NBS} via Thermo Scientific Orion ROSS Ultra pH/ATC Triode combination electrode (8157BNUMD) (± 0.01
422 precision), which was then converted to pH_T and corrected against the other pH_T sensor systems via occasional
423 bottle samples for DIC and TA analysis at NOAA PMEL. Variations between these experiments are noted in
424 Section 3 where necessary and in the Supplementary Materials.

425 [Samples of mineral precipitation were collected as follows: In the tank pH_T 10.3 case, discrete samples of the](#)
426 [precipitate were collected at seven different times after the bulk pH_T value reached 10.3 \(0h, 3h, 24h, 49h, 71h,](#)
427 [145h, 167h - see Fig. 6\) for XRD and SEM analysis. At each timepoint, 0.5 – 1 L seawater was collected from the](#)
428 [tank sampling port and](#) was vacuum filtered through a 0.45 μm Whatman GF/F filter via vacuum pump and the

429 solids were rinsed with DI water 3 times to remove NaCl. The precipitate was dried in an oven at 90 °C, then
430 crushed into a uniform powder via mortar and pestle. Samples were analyzed via Hitachi 4800 Scanning Electron
431 Microscopy (SEM) (5 kV) and Rigaku SmartLab X-ray Diffraction (XRD) (Cu K α , 1.5406 Å, 10 - 100° 2 θ at
432 4°/min) at Brookhaven National Laboratory at the Materials Synthesis and Characterization Facility of the Center
433 for Functional Nanomaterials. We note that material that settled to the bottom of the large tanks was not directly
434 collected, and that only a subset of precipitation was collected at each time point, such that later timepoints may
435 include solids that had precipitated at the beginning of the experiment. Mineral samples from aquaria experiments
436 were collected less frequently due to the volume of seawater required. If precipitation had visibly settled at the
437 bottom of the aquaria, this material was stirred into the water column before sampling from the center of the aquaria.
438 The filtered seawater was immediately analyzed for TA and pH via Ross electrode because the heightened pH was
439 out of the range of spectrophotometric methods. Bottle samples of filtered seawater were not able to be analyzed at
440 NOAA PMEL due to the continued precipitation of CaCO₃ after filtration and preservation.

441 **2.4 Evaluation of CO₂ uptake by seawater in response to NaOH perturbation**

442 ~~Seawater carbonate chemistry measurements were used to analyze the uptake of CO₂ in each tank, primarily relying~~
443 ~~on calculations from the NOAA/PMEL DIC and TA analyses of bottle samples when available and using sensor~~
444 ~~pH_T and Stony Brook TA measurements for cross verification or to fill in between discrete DIC samples. DIC and~~
445 ~~TA data were normalized to the salinity at the start of a given experiment to account for evaporation (Friis et al.,~~
446 ~~2003).~~

447 ~~Carbonate chemistry calculations were then performed using CO2SYS (Lewis and Wallace, 1998), with Luecker et~~
448 ~~al. (2000) carbonate constants, Dickson (1990) for KSO₄, and Lee et al. (2010) for total boron. Wherever possible, a~~
449 ~~combination of CRM analyses and comparisons between simultaneous pH_T sensor and NOAA PMEL bottle samples~~
450 ~~were used to correct SAMI pH and spectrophotometric pH_T sensor data for drift. DIC and TA data were normalized~~
451 ~~to the salinity at the start of a given experiment to account for evaporation (Friis et al., 2003).~~

452 ~~Changes in the seawater carbonate chemistry over time were analyzed with respect to shifts away from the baseline~~
453 ~~within a single control or experiment tank, as well as with respect to the differences between the control and~~
454 ~~experimental tanks.~~

455 **3 Results and Discussion**

456 **3.1 Large tank experiments**

457 A summary of the range of oceanographic variables measured by sensors and bottle samples, calculated via
458 CO2SYS, or extrapolated to equilibration conditions during the large tank experiments is provided in Table 1. This
459 summary includes 6 experiments including 3 targeting pH_T 8.5 (still surface water, with forced air, and with forced
460 air and air bubbling) and one (each) targeting pH_T values of 8.7 (still surface water), 9.5 (with forced air and air
461 bubbling), and 10.3 (still surface water). In two early experiments in which bulk pH_T was raised from the initial
462 condition to 8.3 and to 8.7, the initial pH_T and TA varied between the control and experiment tanks as seawater was
463 pumped from multiple reservoirs and unevenly distributed between the tanks. The experiments were subsequently
464 refined to allow for several days of cross-pumping between tanks to homogenize the control and experiment
465 seawater before NaOH was added at the start of an experiment. More details on experimental variations and a larger
466 summary table are available in the Supplementary Materials. While the initial seawater conditions were similar
467 between the control and experiment tanks, we note that these cases are not entirely comparable after the termination
468 of cross-pumping between tanks and the subsequent addition of alkalinity. While tanks were initially bleached,
469 eventually some biological growth was noted in each tank with potential differences in spatial and temporal
470 distribution as well as species and community differences. Herein, we assume that differences between the control

471 and experiment cases are due to the addition of alkalinity alone, but we note that characterization of other potential
472 confounding factors is a subject for future work.

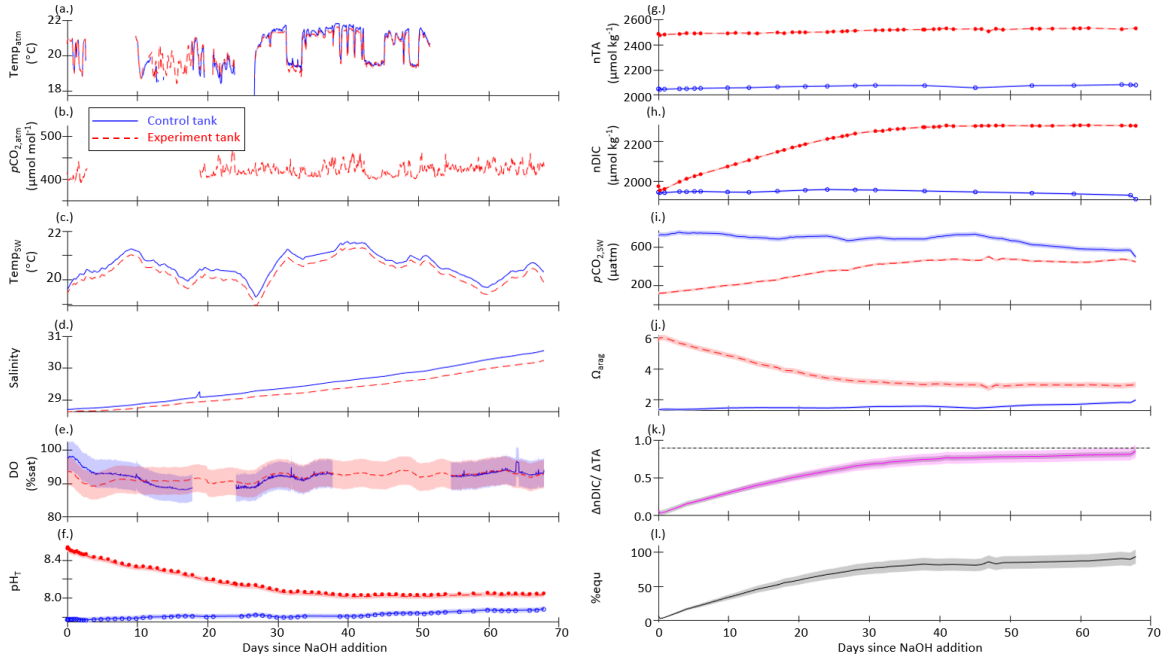
473 The initial pH_T , TA, and DIC varied across experiments as seawater was collected between March 2022 and May
474 2023, ranging from pH_T 7.66 (December 2022) – 7.95 (May 2023), TA 2001 (May 2023) – 2176 (March 2023)
475 $\mu\text{mol/kg}$, and DIC 1847 (May 2023) – 2021 (March 2023) $\mu\text{mol/kg}$. Both measured and CO2SYS -calculated DIC
476 and TA values were normalized to salinity to account for evaporation, which drove salinity increases ranging from
477 0.2 – 7.1 across these experiments.

478 ~~After the addition of NaOH, the control and experiment tanks were allowed to equilibrate with atmospheric CO_2 .~~
479 ~~While refinements in the experimental design allowed for complete or near complete equilibration in later~~
480 ~~experiments, as determined by the stabilization of nDIC at some asymptotic value, early experiments were~~
481 ~~terminated before full equilibration.~~ In all experiments, the absorption of atmospheric CO_2 began immediately after
482 the NaOH addition, as determined by decreasing pH_T and Ω_{arag} and increasing DIC and seawater $p\text{CO}_2$. nTA was
483 fairly stable or increasing (+10 - 60 $\mu\text{mol kg}^{-1}$) after the NaOH addition in all cases except the $\text{pH}_T = 10.3$
484 experiment, where nTA and DIC rapidly decreased due to runaway CaCO_3 precipitation. A stable TA value is an
485 indicator that no significant persistent mineral precipitation (e.g., $\text{Mg}(\text{OH})_2$ or CaCO_3) has occurred. In the absence
486 of active mixing or bubbling, $\text{Mg}(\text{OH})_2$ precipitation occurred immediately upon the introduction of NaOH to
487 seawater, however the precipitation can be rapidly dissolved by turbulence (i.e., pumping NaOH directly above a
488 strong circulation pump and/or stream of air bubbles). No CaCO_3 precipitation was observed in the tanks or aquaria
489 for which the bulk seawater pH_T was <10.0 . The $\text{pH}_T = 10.3$ experiment was designed to induce CaCO_3 runaway
490 precipitation, as described in Section 3.3.

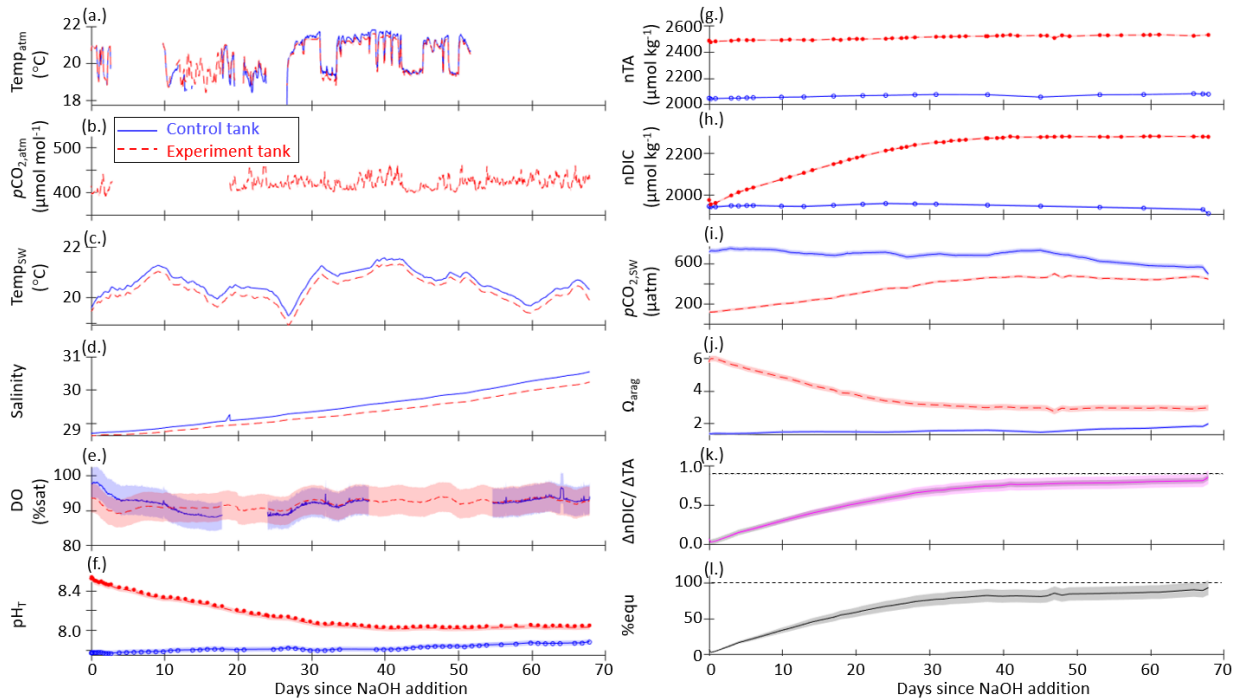
491 Ω_{arag} ranged from 1.4 - 2.5 in the control tanks with minimal variation over the course of any given experiment.
492 During the three experiments in which bulk pH_T was increased to ~ 8.5 , Ω_{arag} increased immediately to 6.0 - 6.3 at the
493 peak of the experiments, before slowly decreasing to 2.8 - 3.0 as the seawater equilibrated with atmospheric CO_2 .
494 For the bulk pH_T 9.5 experiment, Ω_{arag} increased to 20.2 and slowly decreased to 5.0 when the experiment was
495 ended at full equilibration. Mineral precipitation was observed in the bulk pH_T 10.3 experiment, where Ω_{arag} was
496 increased to 30.3 and rapidly (<1 week) fell to 5.2 after the addition of NaOH.

497 The results of one representative set of time-series measurements from the control and experiment tanks are shown
498 in Figure 23 for the case where pH_T of the bulk experiment tank was raised to 8.5 then allowed to relax into
499 equilibration with the atmosphere without the addition of surface air forcing or bubbling. Time-series plots for the
500 other tank-scale experiments are available in the Supplementary Materials.

501



502



503

504

505

506

507

508

509

510

Figure 23: Time-series data for the case where pH_T of the bulk experiment tank was raised to 8.5 with no forced air flow and no bubbling (still surface) for control (blue, solid) and experiment (red, dashed) tanks: (a) continuously measured air temperature, (b) atmospheric $p\text{CO}_2$, (c) seawater temperature, (d) salinity, and (e) dissolved oxygen; (f) pH_T measured by the SAMI-pH (circles) and interpolated from the spec- pH_T (line), corrected to bottle sample and CRM data; (g) NOAA/PMEL-measured TA and (h) DIC from bottle samples and normalized to salinity; (i) seawater $p\text{CO}_2$ and (j) saturation state of aragonite (Ω_{arag}) calculated from interpolated nDIC and nTA data via CO2SYS; (k) the observed carbon uptake ratio (CAR) as $(\text{nDIC}_{\text{exp}} - \text{nDIC}_{\text{control}}) / \Delta\text{TA}_{\text{NaOH addition}}$ (solid) and the theoretical CAR (dashed) from a CO2SYS calculation using measured TA and the average $p\text{CO}_{2\text{atm}}$ to estimate the

511 equilibrium change in DIC (*dashed*); (*l*) the percent equilibration estimated between the observed and theoretical
 512 CAR. Data gaps in panels *a*, *b*, and *e* are due to connectivity issues while offloading sensor data.

513 The ΔnTA and $\Delta nDIC$ values calculated between the control and experiment tanks are summarized in Figure 43;
 514 where nTA and $nDIC$ were interpolated between bottle samples measured at NOAA-PMEL, and/or were calculated
 515 via CO2SYS using sensor pH_T and TA measured at Stony Brook University corrected to less frequent NOAA-
 516 PMEL TA and DIC bottle samples. The ratio of the $\Delta nDIC$ to the addition of alkalinity in the form of NaOH, or
 517 ΔnTA , is included in Figure 4-3 for all experiments except that of the bulk pH_T increase to 10.3. Neglecting
 518 experiments that were terminated before full equilibration, the final observed CAR ranged from 0.75 ± 0.04 to 0.87
 519 ± 0.08 (Table 1).

520 An anomalous event was noted in both the experiment and control cases for the target pH_T 8.5 experiment with
 521 forced air movement across the surface of the tank, wherein an increase in TA and DIC was noted around day 30 of
 522 the experiment. The cause of this event is unclear but could include biological changes in both tanks, the
 523 introduction of alkalinity from environmental contaminants, or the anomalous delayed release of alkalinity from
 524 suspended solids. This event was not observed in any other case, and highlights the importance of using controls to
 525 understand complex interactions in these experiments. A time-series including this event is available in the
 526 Supplementary Materials.

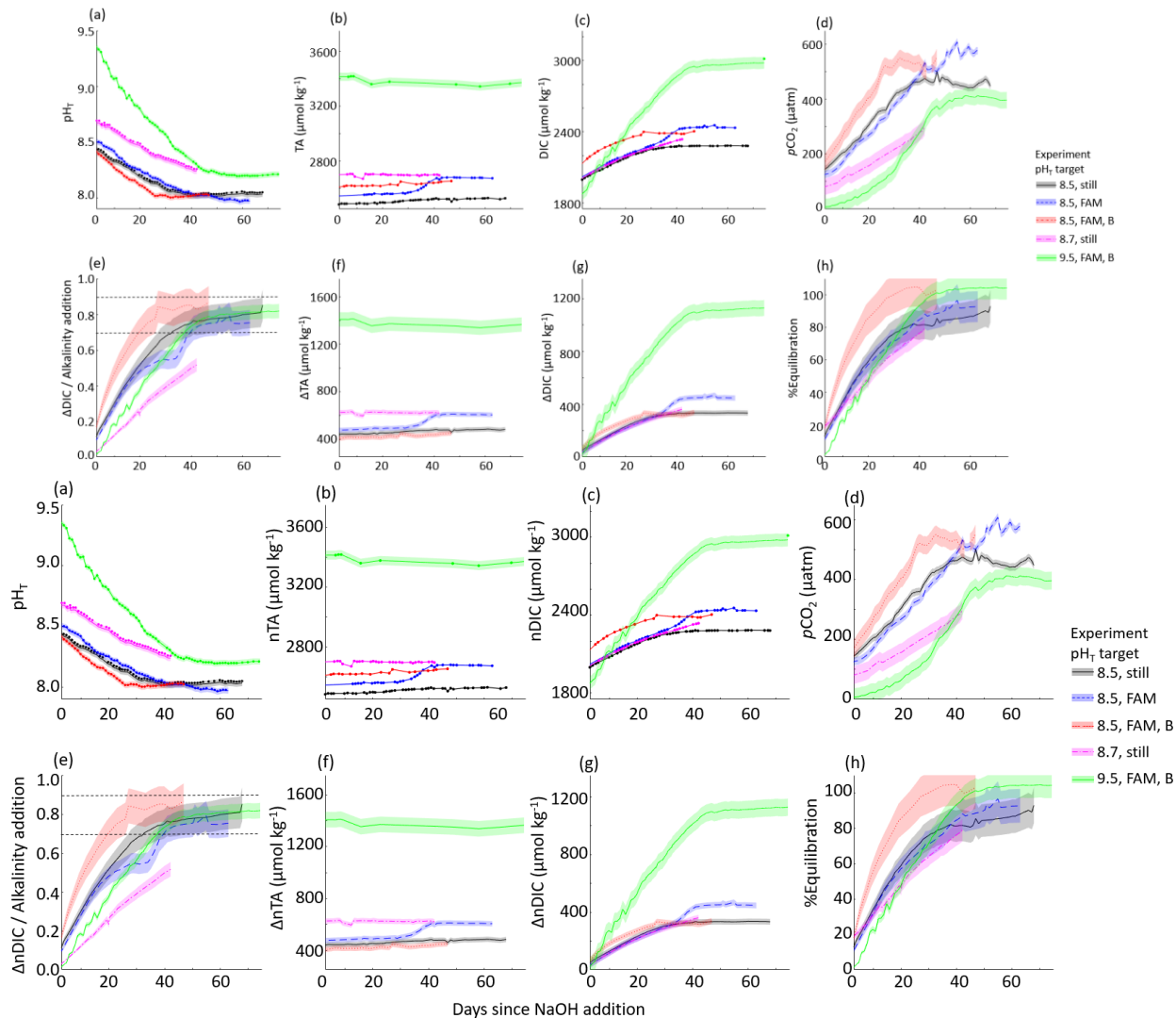
527 ~~Henry's law and CO2SYS calculations were used to estimate the initial and final equilibration condition of each~~
 528 ~~tank experiment. LiCOR $pCO_{2,atm}$ measurements were averaged across experiments to a representative value of 421~~
 529 ~~± 14 ppm, which was used with the initial seawater temperature and salinity to estimate $pCO_{2,seawater}$ at the beginning~~
 530 ~~of each experiment. This The initial CO2SYS-calculated $pCO_{2,seawater}$ was in all cases greater than the atmospheric~~
 531 ~~$pCO_{2,seawater}$, indicating that the seawater was not fully equilibrated with the atmosphere at the time when NaOH was~~
 532 ~~added, likely due to respiration and decomposition of biology removed during the bleaching step (Section 2.1), and~~
 533 ~~as such, the tanks should outgas CO_2 . The initial equilibrium DIC was estimated from a CO2SYS calculation using~~
 534 ~~the $pCO_{2,seawater}$ and nTA_i ; which was in all cases was less than the initial $nDIC$ measured or calculated from nTA_i~~
 535 ~~and $pH_{T,i}$ (by $29 - 108 \mu mol kg^{-1}$). These observations underscore the importance of having a control tank to capture~~
 536 ~~natural dynamics of CO_2 ingassing and outgassing to ensure that changes in DIC attributed to OAE are correctly~~
 537 ~~accounted for.~~

538 ~~The final equilibrium $nDIC$ was estimated from a CO2SYS calculation using the same $pCO_{2,seawater}$ and the nTA~~
 539 ~~measured just after the NaOH addition, corrected for the linear increase in salinity over the course of the experiment.~~
 540 ~~The ratio of the expected $\Delta nDIC$ calculated at equilibrium with the atmosphere to the addition of alkalinity provides~~
 541 ~~a simple estimate of the expected CO_2 storage capacity for a given experiment. The percent equilibration for each~~
 542 ~~experiment was then estimated from the measured and expected values for CAR. Within the series of experiments~~
 543 ~~with a targeted pH_T of 8.5, the timeline to reach an estimated 90% CO_2 equilibration decreased from 65 days (with~~
 544 ~~internal circulation but still water at the surface of the tank), to 50 days (with the addition of forced air movement~~
 545 ~~across the surface of the tank) to 22 days (with the addition of air bubbling). We note that only the two cases~~
 546 ~~(targeted pH_T of 8.5 and 9.5) with the addition of air bubbling reached full equilibration with the atmosphere.~~

547 **Table 1:** Range of variables measured, calculated, or extrapolated in large tank experiments, where M denotes direct
 548 measurement, C denotes calculation via CO2SYS, and E denotes extrapolation to equilibrium conditions. Subscripts
 549 *i* and *f* refer to initial and final conditions, and 'peak' refers to the time point immediately after the addition of
 550 NaOH.

pH_T target	-	8.5	8.5	8.5	8.7	9.5	10.3
Surface condition	-	Still	Forced Air	Forced Air and Air Bubbles	Still	Forced Air and Air Bubbles	Still

Tank (C = control, E = experiment)	-	C	E	C	E	C	E	C	E	C	E	C	E
$\Delta TA = \text{NaOH}$ addition ($\pm 10 \mu\text{mol/kg}$)	M	0	409	0	462	0	375	0	626	0	1406	0	3305
Salinity _i (g/kg)	M	28.7	28.7	30.2	30.2	30.4	30.4	26.9	26.8	26.9	26.9	28.5	28.4
Salinity _f (g/kg)	M	30.5	30.2	37.3	36.6	34.7	33.7	27.6	27.6	29.0	29.2	28.6	28.6
pH _{T,i} (± 0.005)	M	7.76	7.76	7.73	7.73	7.93	7.93	7.92	7.75	7.95	7.95	7.70	7.75
pH _{T,peak} (± 0.005)	M	-	8.54	-	8.58	-	8.49	-	8.68	-	9.51	-	10.10
pH _{T,f} (± 0.005)	M	7.88	8.05	7.85	7.99	7.99	8.01	7.84	8.26	8.01	8.21	7.75	9.52
nTA_i ($\pm 10 \mu\text{mol/kg}$)	M	2049	2049	2069	2069	2248	2248	2075	2075	2007	2007	2023	2025
nTA_{peak} ($\pm 10 \mu\text{mol/kg}$)	M	-	2458	-	2531	-	2623	-	2701	-	3414	-	5330
nTA_f ($\pm 10 \mu\text{mol/kg}$)	M	2080	2528	2235	2674	2246	2624	2095	2696	2014	3363	2041	1253
$nDIC_i$ ($\mu\text{mol/kg}$)	M	1944	1947	1957	1996	2082	2087	1897	1975	1852	1852	1928	1938
$nDIC_f$ ($\mu\text{mol/kg}$)	M	1908	2280	2084	2433	2027	2365	1937	2336	1832	2977	1947	720
$\Omega_{\text{aragonite},i}$	C	1.39	1.37	1.4	1.1	2.0	2.0	2.4	2.4	1.9	1.9	1.4	1.3
$\Omega_{\text{aragonite,peak}}$	C	-	5.9	-	6.0	-	6.2	-	8.8	-	19.3	-	30.3
$\Omega_{\text{aragonite},f}$	C	2.0	3.0	1.7	2.8	2.5	3.0	1.9	4.4	2.1	4.9	1.4	5.2
CAR _f	C	-	0.85 ± 0.04	-	0.75 ± 0.04	-	0.87 ± 0.08	-	0.52 ± 0.07	-	0.82 ± 0.09	-	-
CAR _{equilibrium}	E	-	0.89	-	0.85	-	0.85	-	0.84	-	0.81	-	-
% equilibration (time elapsed in days)	E	-	95 ± 10 (67)	-	92 ± 10 (63)	-	102 ± 12 (45)	-	79 ± 6 (42)	-	104 ± 7 (74)	-	(13)



551

552

553 **Figure 34:** Results of 5 tank-scale experiments in which enough NaOH was added to each tank to raise the bulk pH_T
 554 to 8.3 – 9.7. pH_T decreased rapidly in all cases in which air bubbling sped equilibration with atmospheric CO_2 .
 555 Results include: (a) measured pH_T , (b) measured $\bar{n}\text{TA}$, (c) measured $\bar{n}\text{DIC}$ or CO_2SYS calculated (for pH_T 9.5 case
 556 only), (d) CO_2SYS -calculated pCO_2 , (e) the observed carbon uptake ratio (CAR) as $(\bar{n}\text{DIC}_{\text{exp}} - \bar{n}\text{DIC}_{\text{control}}) / \Delta\bar{n}\text{TA}_{\text{NaOH addition}}$ with horizontal dashed lines representing the expected range of 0.7-0.9 mol CO_2 uptake / mol NaOH
 557 added to seawater, the change in (f) $\bar{n}\text{TA}$ and (g) $\bar{n}\text{DIC}$ compared to the baseline measurements before the addition
 558 of NaOH, and the percent equilibration estimated between the observed and theoretical CAR.
 559

560 3.2 Aquaria experiments

561 *The large volume of tank experiments allowed for precise measurement of the seawater carbonate chemistry via*
 562 *bottle sampling (1L each, sent to NOAA/PMEL for analysis) with high sampling frequency. To compliment these*
 563 *measurements, we also performed a series of experiments in smaller aquaria (15 L each), which enabled a larger*
 564 *number of replicates and a faster time to equilibrium when bubbled with air.* Table 2 provides a summary of the
 565 range of oceanographic variables quantified for the aquaria experiments.

566 **Table 2:** Range of variables measured, calculated, or extrapolated in aquaria experiments, where M denotes direct
 567 measurement, C denotes calculation via CO2SYS, and E denotes estimation within specified equilibration
 568 conditions. Subscripts *i* and *f* refer to initial and final conditions, and ‘peak’ refers to the time point immediately
 569 after the addition of NaOH.

pH _T target	-	0 Control	8.3	8.5	8.5 Without air bubbles	8.7	9.3	9.5	9.7	9.9	10.0	10.1	10.2	10.3
ΔTA = NaOH addition (± 10 μmol/kg)	M	0	187	331	362	543	1409	1679	2037	2216	2276	2504	2796	3829
pH _{T,i} (± 0.1005)	M	7.94	7.97	7.90	7.86	7.95	7.98	7.98	7.98	8.06	8.04	8.04	8.04	7.95
pH _{T,peak} (± 0.1005)	M	-	8.28	8.41	8.40	8.63	9.22	9.43	9.64	9.83	9.91	10.23	10.32	10.20
pH _{T,f} (± 0.1005)	M	8.06	8.03	8.07	8.11	8.08	8.21	8.209.0 2	8.23	8.65	8.96	8.72	9.46	7.99
TA _i (± 10 μmol/kg)	M	2265	2262	2250	2250	2250	2393	2393	2393	2531	2531	2531	2531	2250
TA _{peak} (± 10 μmol/kg)	M	-	2449	2582	2611	2793	3801	4072	4430	4748	-	-	-	4608
TA _f (± 10 μmol/kg)	M	2323	2476	2640	2645	2822	3837	4110	4420	4462	1702	1835	1537	2202
DIC _i (μmol/kg)	C	2089	2073	2091	2107	2070	2192	2192	2192	2282	2287	2287	2287	2067
DIC _f (μmol/kg)	C	2113	2246	2377	2382	2540	3372	3486	3877	3389	992	1244	671	2003
Ω _{aragonite,i}	C	2.1	2.2	1.9	1.8	2.1	2.34	2.4	2.4	2.9	2.8	2.8	2.8	2.1
Ω _{aragonite,peak}	C	-	4.2	5.5	5.5	8.1	19.5	23.1	27.0	29.8	30.2	30.9	32.4	38.9
Ω _{aragonite,f}	C	2.4	2.7	3.1	3.1	3.4	5.9	7.9	7.1	13.7	6.5	5.7	7.0	2.2
CAR _f	C	-	0.92 ± 0.10	0.87 ± 0.06	0.76 ± 0.05	0.87 ± 0.04	0.84 ± 0.02	0.86 ± 0.02	0.84 ± 0.02	0.50	-	-	-	-
CAR _{equilibrium}	E	-	0.69	0.67	0.64	0.77	0.80	0.80	0.80	0.81	-	-	-	-
% equilibration (time elapsed in days)	E	(40)	130 (16)	126 (18)	116 (40)	111 (16)	104 (18)	106 (18)	104 (18)	62 (1)	(1)	(1)	(1)	(16)
CaCO ₃ precipitation?	M	-	No	No	No	No	No	No	No	No	Yes	Yes	Yes	Yes

570 The aquaria experiments are not directly comparable to the control stated in Table 2. One Seawater for one control
 571 aquarium was collected in March 2023, and was monitored for pH_T and TA changes beginning in March 2023 and
 572 concluding in through May 2023. This is because sSeawater for these the experimental aquaria experiments was
 573 collected in three batches between March, April, and and May 2023, with only 4-6 aquaria experiments running in
 574 parallel within each set of experiments due to space and analytical throughput constraints. Because of this, the
 575 experiments started in March 2023 could be compared directly to the control (target pH_T 8.3, 8.5, 8.5 still, and 8.7);
 576 but the rest of the experiments used different initial seawater than the control aquaria. One control aquarium was
 577 monitored for pH_T and TA changes beginning in March 2023 and concluding in May 2023. The CAR for each
 578 aquaria experiment was therefore calculated from changes in DIC and TA between the initial ‘baseline’ condition
 579 and after the NaOH was added within a given aquarium, rather than between the experiment and control cases. The
 580 CAR ranged between 0.76 ± 0.05 and 0.92 ± 0.10, excluding cases where mineral precipitation was evident and for
 581 the pH_T 9.9 case where the experiment ended after one day due to a sensor logging failure. This wide range in
 582 ΔDIC/ ΔTA is likely due to the lack of a control for aquaria experiments, low temporal resolution of limited number
 583 of pH_T and TA samples collected throughout these experiments (daily at best with no duplicates due to the limited
 584 volume) samples, and the imprecision of electrode-based pH_T measurements relative to the SAMI-pH and spec-pH_T
 585 based measurements used in the large tank experiments.

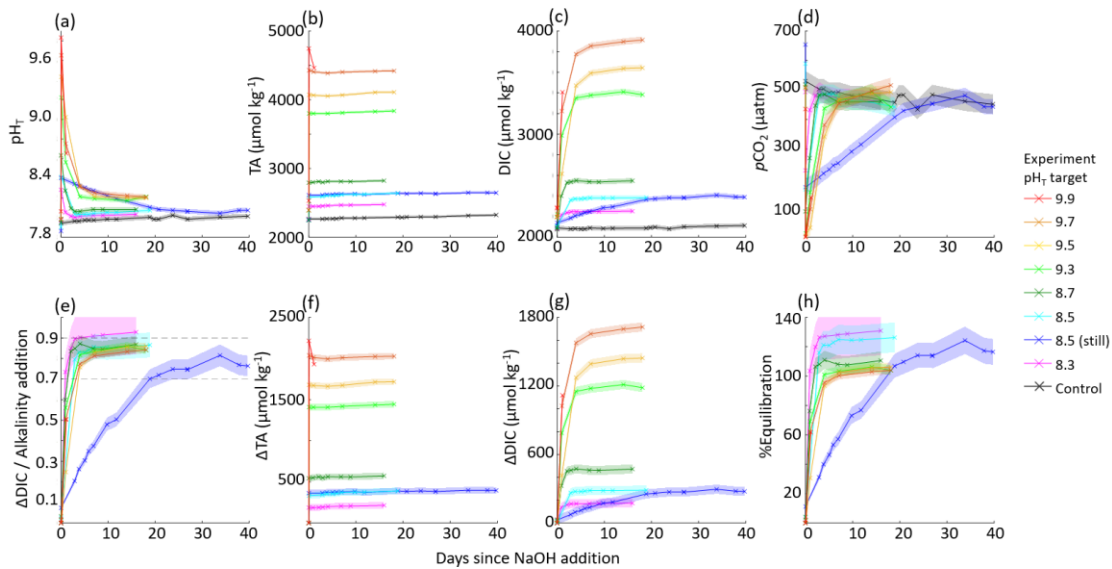
586 With the exception of a single target $\text{pH}_T 8.5$ experiment, all aquaria were bubbled with ambient air, allowing for
587 rapid CO_2 exchange, and an optically clear lid was placed on each aquarium to reduce evaporation and splashing
588 onto nearby equipment. Some evaporation was evident from the rising TA throughout these experiments, but was
589 not resolvable within the resolution of a handheld salinometer used for these experiments, which ranged from values
590 of 30 – 31 during the experiments. Therefore, DIC and TA were not normalized to salinity in these cases.
591 Temperature was discretely recorded from a combination Ross pH electrode, and temperature values ranged from 19
592 – 21 °C during the experiments.

593 The initial CO2SYS-estimated equilibrium DIC was in all cases less than the initial DIC calculated from TA_i and
594 $\text{pH}_{T,i}$ (by 16 – 36 $\mu\text{mol kg}^{-1}$). This indicates that the seawater was not fully equilibrated with the atmosphere at the
595 time when NaOH was added, likely due to respiration and decomposition of biology removed during the bleaching
596 step (Section 2.1), and as such, the aquaria would be expected to outgas CO_2 if NaOH were not added. Absorption
597 of atmospheric CO_2 began immediately after the NaOH addition, as determined by decreasing pH_T . We note that
598 there are significant uncertainties in these equilibrium estimates leading to estimates of >100% equilibration. These
599 estimates would be better constrained with more continuous carbonate chemistry measurements, particularly
600 seawater and atmosphere $p\text{CO}_2$ throughout the experiments that would allow for more direct calculation of air-sea
601 CO_2 flux and equilibration, and finer control of bubbling and diffusion rates are necessary to define the timeline for
602 equilibration within the aquaria.

603 After the addition of NaOH, the aquaria were allowed to equilibrate with atmospheric CO_2 . Similar to the large tank
604 experiments, we used Henry's law and CO2SYS calculations to estimate the initial and final equilibration condition
605 of each aquaria experiment. The same average $p\text{CO}_{2,\text{atm}}$ of 421 ± 14 ppm was used with the initial seawater
606 temperature and salinity to estimate $p\text{CO}_{2,\text{seawater}}$ at the beginning of each experiment. The initial equilibrium DIC
607 was estimated from a CO2SYS calculation using this $p\text{CO}_{2,\text{seawater}}$ and TA_i , which in all cases was less than the initial
608 DIC calculated from TA_i and $\text{pH}_{T,i}$ (by 136 – 36 $\mu\text{mol kg}^{-1}$). This indicates that the seawater was not fully
609 equilibrated with the atmosphere at the time when NaOH was added, likely due to respiration and decomposition of
610 biology removed during the bleaching step (Section 2.1), and as such, the aquaria should would be expected to
611 outgas CO_2 if NaOH were not added. The final equilibrium DIC was estimated from a CO2SYS calculation using
612 the same $p\text{CO}_{2,\text{seawater}}$ and the TA measured just after the NaOH addition. The percent equilibration for each
613 experiment was then estimated between the measured and predicted values for $\Delta\text{DIC}/\Delta\text{TA}$. Due to the air bubbling,
614 most experiments approached equilibrium with the atmosphere within 1–7 days, with the exception of the non-
615 bubbled $\text{pH}_T 8.5$ experiment that took ~20 days. The surface water of this non-bubbled experiment was stagnant, and
616 the water was only mixed via stirring just before taking pH_T and TA samples. Absorption of atmospheric CO_2 began
617 immediately after the NaOH addition, as determined by decreasing pH_T . We note that there are significant
618 uncertainties in these equilibrium estimates leading to estimates of >100% equilibration., and that mThese estimates
619 would be better constrained with more continuous seawater carbonate chemistry measurements, particularly
620 seawater and atmosphere $p\text{CO}_2$ throughout the experiments that would allow for more direct calculation of air-sea
621 CO_2 flux and equilibration, and finer control of bubbling and diffusion rates are necessary to define the timeline for
622 equilibration within the aquaria.

623 Each aquaria was gently stirred during the addition of NaOH to prevent $\text{Mg}(\text{OH})_2$ precipitation. No CaCO_3
624 precipitation was observed in the tanks below a bulk seawater pH_T of 10.0, and TA remained stable in each of these
625 experiments with the exception of some increase driven by minor evaporation on the order of +2 $\mu\text{mol/kg}$ per day.
626 Experiments where CaCO_3 precipitation was induced by increasing the starting pH_T to values above 10 are
627 discussed in Section 3.3.

628 The aquaria experiments with target pH_T from 8.3 – 9.9 are summarized in Figure 45.



629

630 **Figure 45:** Results of 9 aquaria experiments in which enough NaOH was added to each aquaria to raise the bulk
 631 pH_T to 8.3 – 9.9. pH_T decreased rapidly in all cases in which air bubbling sped equilibration with atmospheric CO_2 .
 632 Results include: (a) measured pH_T , (b) measured TA, (c) CO2SYS-calculated DIC, (d) CO2SYS-calculated pCO_2 ,
 633 (e) the observed carbon uptake ratio (CAR) as $(DIC_{exp} - DIC_{baseline}) / \Delta TA_{NaOH\ addition}$ with horizontal dashed lines
 634 representing the expected range of 0.7-0.9 mol CO_2 uptake / mol NaOH added to seawater, the change in (f) TA and
 635 (g) DIC compared to the baseline measurements before the addition of NaOH, and the percent equilibration
 636 estimated between the observed and theoretical CAR.

637 In general, the large tanks and aquaria showed reasonable agreement in achieving values for CAR within the
 638 expected range of 0.7-0.9 (He and Tyka, 2023; Burt et al., 2021; Wang et al., 2023). While the use of aquaria
 639 bubbled with air to speed equilibration allowed for a greater range of data collection within a constrained experiment
 640 timeline, the quality of this data is limited by the lack of appropriate sensors to fit into these small 15 L aquaria,
 641 challenges with establishing control conditions, and fewer bottle samples due to the reduced quantity of seawater.
 642 However, while the large tanks allow for a larger range of oceanographic sampling and sensing techniques, it is
 643 more challenging to fully quantify mixing and circulation rates in the current large tank experimental setup.

644 Figure 56 shows the dependence of the equilibrium values of ΔDIC , CAR, and $\Delta pH_T = (pH_{final} - pH_{initial})$ as a
 645 function of the target starting pH_T value after alkalinity addition for both tank and aquaria experiments in which the
 646 final percent equilibration for CO_2 was estimated at greater than 90%. Higher starting pH values correspond to a
 647 greater alkalinity addition Results for tank and aquaria experiments aligned well, with increasing, resulting in larger
 648 values of ΔDIC for increasing alkalinity additions relative to lower starting pH values. The CAR was observed for
 649 all experiments to fall within the range typical-expected for seawater with the temperature and salinity values used in
 650 these tests. As expected from calculations of the response of the seawater carbonate buffer system to additions of
 651 alkalinity, the final pH_T at equilibrium exceeded the initial pH_T value of the control tank or aquaria at the same
 652 time point prior to the addition of alkalinity. That is, even once equilibrium in the alkalinity enhanced experiment
 653 tank had been reached, the ending pH value was slightly elevated relative to both the starting pH_T value and the
 654 pH_T of the control. While not all of these experiments resulted in complete equilibration, a line fit to the aquarium
 655 experiments has a slope of 0.0001 which is ??-compared similar to the slope of the line that is expected from
 656 CO2SYS when assuming complete equilibration with a 421 ppm CO_2 atmosphere. This finding warrants further
 657 investigation on the potential of OAE to mitigate some acidification impacts in controlled field trials by metering the
 658 discharge of alkalinity to semi-protected water body.

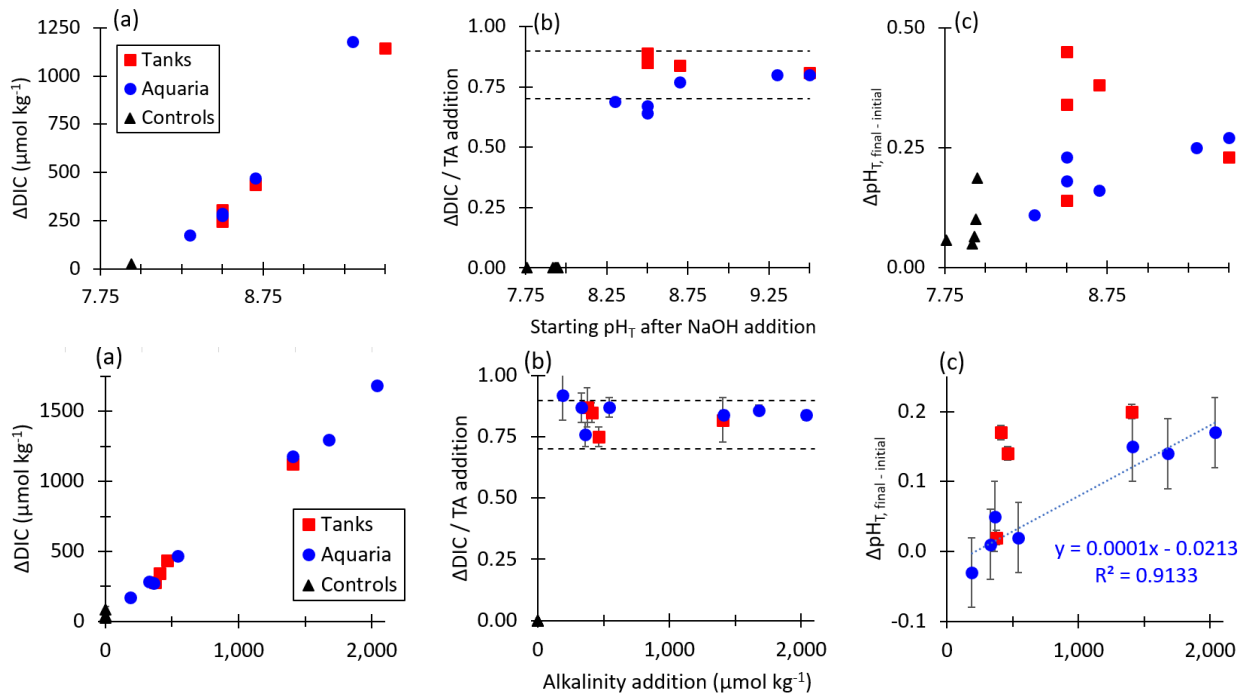


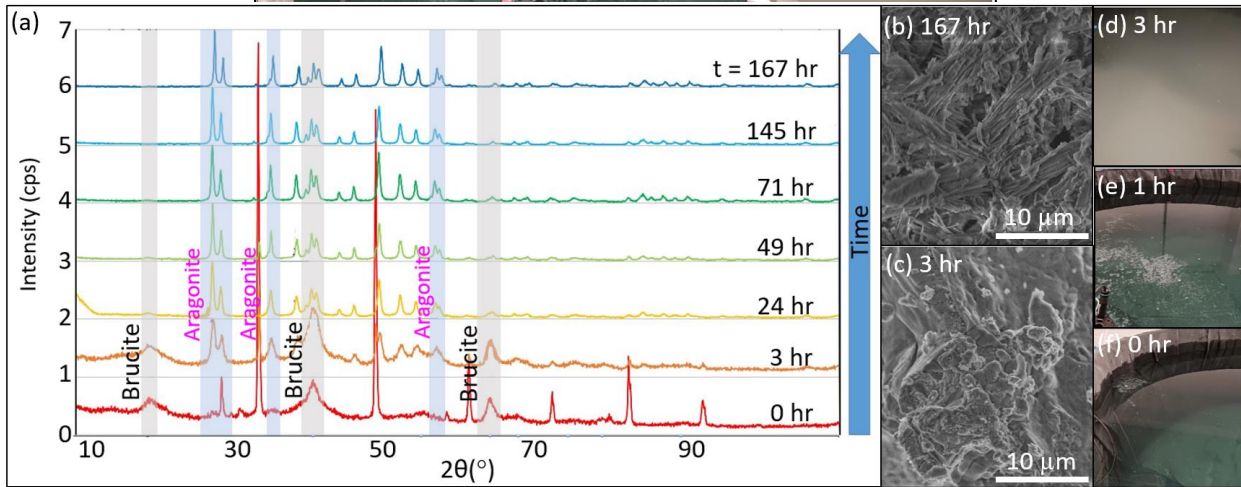
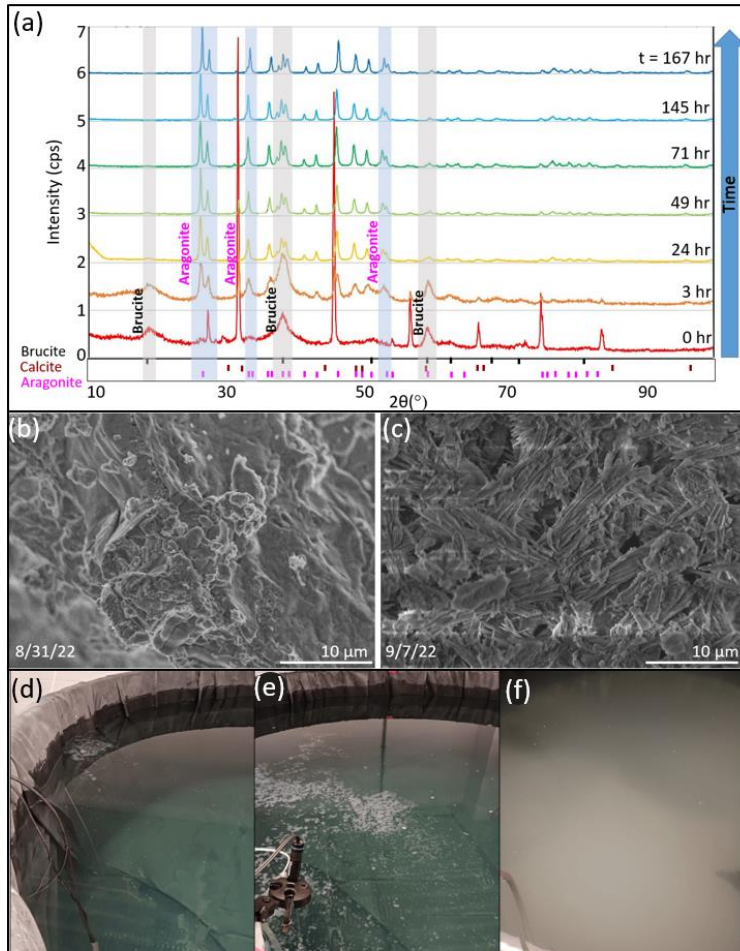
Figure 56: (a) The change in final CO₂SYS-predicted DIC relative to the initial conditions for tank, aquaria, and control experiments increases with increasing NaOH additions for cases where the air-sea CO₂ equilibration was estimated at >90% at the termination of each experiment. (b) CO₂SYS-predicted CAR (Δ DIC / Alkalinity addition) at air-sea equilibrium conditions for tank, aquaria, and control experiments, with horizontal dashed lines representing the expected range of 0.7-0.9 mol CO₂ uptake / mol NaOH added to seawater. (c) The CO₂SYS-predicted-measured Δ pH_T = (pH_{final, experiment} - pH_{final, control}) increases as a function of the target pH_T value after with alkalinity addition for both tank and aquaria experiments.

3.3 Experiments exceeding the CaCO₃ precipitation threshold

While Mg(OH)₂ precipitation occurs immediately upon introduction of concentrated (i.e., ~0.5 M) NaOH to still seawater, it may be rapidly dissolved or avoided entirely by gentle mixing, including via the use of stirrers, circulation pumps, or air bubblers. This precipitation and redissolution happened rapidly enough that it was not identified in any TA or other variables measured in the aquaria and tank tests. However, in cases where enough NaOH was added to raise the bulk seawater pH_T to greater than 10.0 (i.e., in one large tank test with a target pH_T of 10.3, and in 4 aquaria experiments ranging from pH_T 10.0-10.3), runaway precipitation of Mg(OH)₂ and CaCO₃ was observed. This was characterized by a sharp reduction in both TA and DIC and an increase in turbidity, and a continued depletion of DIC and slow removal of TA as atmospheric CO₂ from gas exchange was converted to additional CaCO₃. Runaway precipitation has been described as a condition in which more alkalinity is removed from seawater by mineral precipitation than was initially added until a new steady state is achieved (Moras et al., 2022; Hartmann et al., 2023; Suitner et al., 2023). This can significantly impact reduce the efficiency of OAE, and has implications for biological productivity, as increased turbidity may impact photosynthesis or predator-prey interactions.

In both the tank and aquarium pH_T 10.3 cases, discrete samples of the precipitate were collected at seven different times after the bulk pH_T value reached 10.3 (0h, 3h, 24h, 49h, 71h, 145h, 167h—see Fig. 6) for XRD and SEM analysis. At each timepoint, 0.5—1 L seawater was collected from the tank sampling port or from the center of the aquaria. In cases where precipitation had visibly settled at the bottom of the aquaria, this material was stirred into the water column before sampling. We note that material that settled to the bottom of the large tanks was not directly

687 ~~collected, and that only a subset of precipitation was collected at each time point, such that later timepoints may~~
688 ~~include solids that had precipitated at the beginning of the experiment. The filtered seawater was immediately~~
689 ~~analyzed for TA and pH via Ross electrode because the heightened pH was out of the range of spectrophotometric~~
690 ~~methods. Bottle samples of filtered seawater were not able to be analyzed at NOAA PMEL due to the continued~~
691 ~~precipitation of CaCO₃ after filtration and preservation.~~ Both XRD and SEM results of the mineral precipitation
692 showed the dominance of Mg(OH)₂ precipitation immediately after the alkalinity addition and the corresponding
693 increase in pH and $\Omega_{\text{aragonite}}$ (to a value of around 30), though this signal was partially obscured by the presence of
694 other salts. The Mg(OH)₂ precipitation at this stage was thick, slurry-like, and difficult to appropriately rinse. Within
695 hours of the NaOH addition, the runaway CaCO₃ precipitation began, characterized by fine, light particulates in the
696 water column and a sharp increase in turbidity. Within ~24 hours of the NaOH addition, most Mg(OH)₂ signals had
697 disappeared, leaving only aragonite and calcite peaks in the XRD. The results of the XRD analysis for the tank
698 experiment are summarized in Figure 7, and the aquarium experiment showed similar results. TA decreased
699 throughout the precipitation of Mg(OH)₂ and CaCO₃, and was below that of the initial seawater within 24 hours of
700 the NaOH addition. In the tank experiment, the initial TA (2025 $\mu\text{mol/kg}$) was raised by 3305 $\mu\text{mol/kg}$. Within 3
701 days the TA had decreased to 1583 $\mu\text{mol/kg}$ and continued to decrease through the termination of the experiment to
702 1253 $\mu\text{mol/kg}$ 10 days after the addition of NaOH. The DIC, which was initially measured ~~at to be~~ 1938 $\mu\text{mol/kg}$,
703 decreased to 720 $\mu\text{mol/kg}$ by the end of the experiment. This experiment shows that runaway CaCO₃ can result in a
704 significant loss of both efficiency of alkalinity dosing for OAE projects and of storage of carbon in the form of DIC.
705 A figure of time-series data collected during the tank experiment is available in the supplementary-Supplementary
706 materialsMaterials.



707

708

709 **Figure 67:** (a) XRD analysis (top) of particulates filtered from seawater after the addition of enough NaOH to raise
 710 the bulk seawater pH_T to 10.3 showed mineral precipitation initially dominated by $\text{Mg}(\text{OH})_2$ before it was overtaken
 711 by $\text{CaCO}_{3,\text{arag}}$. The shaded grey vertical bars highlight peaks characteristic of brucite which typically disappear after
 712 24 hours, and the shaded blue bars represent several aragonite peaks which appear between 3 and 24 hours.
 713 Representative SEM images show (b) $\text{CaCO}_{3,\text{arag}}$ at the end of the experiment, $\text{Mg}(\text{OH})_2$ captured ~3 hours after the
 714 NaOH addition, and (c) $\text{Mg}(\text{OH})_2$ captured ~3 hours after the NaOH addition, $\text{CaCO}_{3,\text{arag}}$ at the end of the experiment.

715 Photographs of the tank experiment show seawater (d) ~~before NaOH addition~~ ~3 hours after the NaOH addition,
716 when runaway CaCO₃ precipitation became visually apparent, (e) during NaOH addition into still water (i.e.,
717 without the use of stirrers, circulation pumps, or air bubblers to break up and redissolve Mg(OH)₂), and (f) ~~before~~
718 NaOH addition ~~~3 hours after the NaOH addition, when runaway CaCO₃ precipitation became visually apparent.~~

719 In summary, the presence and duration of brucite precipitation upon addition of 0.5 M aqueous NaOH depends on
720 the ratio of the NaOH addition rate to the local dilution rate in the receiving waters. Future research using flow
721 through tanks could help identify thresholds below which brucite precipitation can be avoided or limited, and the
722 immediate formation of Mg(OH)₂ may be reversible, as also noted by Suitner et al. (2023) and Cyronak et al.
723 (2023). At the given initial seawater conditions, the threshold for aragonite precipitation began ~~at~~ at an Ω_{arag} of 30,
724 corresponding to $\text{pH}_T > 10.0$, and continued as Ω_{arag} decreased to ~ 5.2 . This threshold corresponded to an increase in
725 TA of $> 2270 \mu\text{mol/kg}$. The potential for runaway aragonite this precipitation may be reduced by active mixing at the
726 point of NaOH introduction, maintaining a mixing volume below bulk seawater pH_T of 10.0, and allowing for
727 appropriate dilution in flow-through conditions, particularly on timescales of hours after alkalinity addition.

728 ~~Additional~~ Characterization of runaway precipitation thresholds at varying temperatures, salinities, and suspended
729 particulate conditions will allow for OAE implementation designs that best avoid this potential risk to OAE
730 efficiency and ecosystem perturbation. We note that these results are only valid for open experiments using an
731 aqueous hydroxide feedstock for alkalinity, and may not be comparable to bench-scale experiments such as closed
732 bottle incubations, where increased surface area, edge effects, and sustained conditions of high Ω_{arag} may result in
733 precipitation at different thresholds. We also note that we do not assume zero aragonite precipitation at conditions
734 below the stated thresholds, but that potential precipitation is not readily detectable with our experimental setup. For
735 example, heterogeneous CaCO₃ precipitation events, such as may occur on suspended sediments in the water
736 column, have been suggested through characteristic changes in seawater TA/DIC ratios in cases of riverine inputs
737 and bottom sediment resuspension (Bustos-Serrano et al., 2009; Wurgaft et al., 2016; 2021). Suspended sediments in
738 the context of OAE project sites could influence OAE efficiency and the potential for runaway precipitation and
739 should be included in future studies (Bach, 2023). The thresholds determined in this study are significantly higher
740 than those of some mineral-based OAE studies, including precipitation after an increase in TA of $\sim 500 \mu\text{mol/kg}$
741 using CaO and Ca(OH)₂ mineral additions (Moras et al., 2022). Hartmann et al. (2022) noted precipitation resulting
742 from alkalinity additions of $> 600 \mu\text{mol/kg}$ Mg(OH)₂, and found that aqueous alkaline solutions avoided carbonate
743 precipitation better than reactive alkaline particle additions to seawater. Suitner et al. (2023) suggested that alkalinity
744 additions $> 2000 \mu\text{mol/kg}$ could be achievable given sufficient dilution to avoid runaway precipitation. Together,
745 these studies highlight the need to expand research into runaway precipitation to characterize potential inefficiencies
746 in OAE, particularly in in-situ experiments to establish relationships applicable to ocean environments.

747 5 Summary

748 These results demonstrate that ocean alkalinity enhancement using aqueous sodium hydroxide in seawater results in
749 CO₂ removal from air at an efficiency of 0.75 (± 0.04) – 0.92 (± 0.10), with 90% equilibration typically achieved
750 within 7 - 9 weeks (still surface water with ~ 16 L/min subsurface circulation through UV arrays) to 3 - 5 weeks
751 (with the addition of ambient air bubbling into the bottom of each tank) of the initial addition when performed in
752 ~ 6000 L tanks with seawater-air contact areas of around 4.6 m². These results are in general agreement with ratios
753 noted in Burt et al. (2021), He and Tyka (2023), and Wang et al., (2023), and thus give no reason to doubt the air-sea
754 equilibrium dynamics used in these model based OAE studies. Here, uncertainties are driven by sensor precision and
755 temporal resolution in discrete DIC and TA sampling, the limited number of experiments with minimal
756 opportunities for duplicates or replicates, and poorly constrained data on mixing, circulation, and air bubbling rates.
757 Ongoing experiments seek to improve each of these conditions and should particularly focus on constraining the
758 movement of water within a given tank to improve air-sea equilibration estimates and to allow for better
759 extrapolation from tank to field experiments. In addition, a focus of ongoing and future work is to provide rate

760 estimates for the uptake of atmospheric CO₂ in response to an NaOH addition, allowing for fitting and extrapolation
761 of a shortened experiment to equilibration with the atmosphere. While the tank-to-atmosphere exchange rate is
762 unlikely to be generalizable to the ocean sea-to-air kinetics, it is essential information for the storage of high TA
763 solutions (which will be a common element of many OAE field trials) and for the subset of proposed approaches
764 that plan to conduct partial pre-equilibration of high-TA seawater mixtures before discharge (typically to avoid
765 creating high-pH environmental conditions).

766 We relied on several methods to constrain seawater carbonate chemistry. The tank-scale experiments primarily
767 relied on discrete (at most ← daily) DIC and TA sampling (NOAA PMEL), paired with daily measurements from
768 spectrophotometric pH systems (SAMI-pH and a semi-automated benchtop spec-pH system following Carter et al.
769 (2013)) and local TA measurements. With appropriate calibration or correction of the spec-pH systems relative to
770 CRM, there was no significant difference in carbonate calculations using the NOAA PMEL DIC-TA or spec-pH-
771 local TA pairings, though the latter case typically produced larger uncertainties. Aquaria experiments relied on a
772 standard glass pH electrode (at most ← daily, corrected to spectrophotometric systems) with discrete (at most ← daily)
773 TA measurements, which provided reasonable data relative to the tank experiments. As a result, ongoing tank-scale
774 experiments have limited the volume of discrete DIC and TA samples collected for analysis at NOAA PMEL to
775 allow for faster and less expensive monitoring via spec-pH and local TA titrations. However, we note that the major
776 limitation in this measurement pathway lies in the spec-pH method, which is typically limited to pH_T measurements
777 ranging from 7 – 9 for the meta-cresol purple indicator dye used. While our measurements retained some sensitivity
778 up to pH_T 9.5, such a method should typically be considered unreliable at these pH_T values, and we relied on
779 frequent correction to CRM and comparison with DIC/TA samples. Thymol blue is an alternative
780 spectrophotometric pH_T indicator dye with sensitivity over the higher pH_T conditions observed during these initial
781 trials and will be assessed for future experiments ([Zhang and Byrne, 1996](#); [Liu et al., 2006](#)).

782 Aqueous NaOH with concentrations as high as 0.5 M can be added directly to turbulent seawater with only limited
783 observable precipitation of Mg(OH)₂. In these conditions this precipitated mineral rapidly redissolves on the
784 timescales of minutes to seconds. Improved control over the NaOH dosing rate (in our tank experiments, ~50 mL
785 NaOH/min) and the turbulence of the receiving water through metered flow through experiments will be valuable in
786 extrapolating to field conditions. This precipitation is detectable both visually and through turbidity measurements
787 and implies that straightforward measurement of pH and turbidity at the dispersal site can be used to adjust the
788 alkalinity dispersal rate according to local mixing conditions such that Mg(OH)₂ precipitation is avoided and/or
789 redissolves when it occurs. No significant CaCO₃ precipitation was observed at pH <10.0 or Ω_{aragonite} < 30.0.
790 Runaway CaCO₃ precipitation was observed above these thresholds, where a massive precipitation and settling of
791 Mg(OH)₂ and CaCO₃ solids results in less alkalinity in the overlying water than at the starting condition. pH and
792 turbidity sensing combined with discrete TA measurements could be used as a feedback signal for alkalinity dosing
793 into seawater to ensure that the local maximum thresholds at the dispersal location do not approach or exceed
794 conditions that promote significant CaCO₃ precipitation. We note that future investigations seeking to better
795 approximate field conditions should take into account seasonal and tidal shifts in temperature and salinity, and
796 varying conditions of suspended sediment in the water column, including that of aerial dust, terrestrial runoff, and
797 resuspended bottom sediments.

798 In these experiments, the seawater was filtered and bleach treated prior to experiments to limit biological growth,
799 and both tank and aquaria experiments were conducted indoors with limited light. Nevertheless, in most
800 experiments, biological growth was observed after a few weeks, including cyanobacteria and coccolithophores. A
801 series of experiments are underway to test the difference in CO₂ removal efficiency for two side-by-side tanks, both
802 of which are dosed with NaOH, but only one of which was bleached. Preliminary results show minimal difference
803 between the bleached and unbleached tanks, indicating these experiments are applicable to real-world conditions, at
804 least for regions with biological communities similar to that of Long Island Sound, but further investigation is
805 warranted.

806 A focus of future work is to consider the potential impact of [electrochemical OAE](#) ~~the SEAMATE process~~ on local
807 ocean acidification mitigation efforts. We note that in each constrained tank and aquaria experiment, the pH_T at
808 equilibrium exceeds the initial pH_T value prior to the addition of alkalinity ([see Fig. 5c](#)). A controlled release of
809 alkalinity could theoretically be configured to maintain a locally elevated pH_T value relative to pre-alkaline
810 conditions, with potential uses in aquaculture and hatchery environments.

811 These results provide clear and practical guidelines for MRV for OAE implementations employing aqueous
812 alkalinity. First, carbonate chemistry and turbidity measurements at the alkalinity dispersal location can ensure that
813 seawater parameters such as pH and $\Omega_{\text{aragonite}}$ remain within pre-determined safe bounds and that unwanted
814 precipitation is avoided. Second, for a given OAE deployment, where ocean models provide a reasonable certainty
815 about the fraction of the alkalinity plume remaining in the surface over weeks to months, the CO_2 removal efficiency
816 and timescale for air-seawater equilibration provided by our [shallow-depth](#) experiments can place an [lower-upper](#)
817 bound on the amount of CO_2 removal expected from that OAE intervention. Expanding these studies from tank scale
818 to mesocosm and field experiments will be crucial to understanding biological impacts and constraining realistic air-
819 sea interactions in response to this type of OAE ([Oschlies et al., 2023](#)).

820 **Data availability**

821 Data are described in the manuscript and provided Supplementary Materials, which includes a .csv file with
822 processed sensor and sample time-series data at hourly resolution.

823 **Author contribution**

824 MDE and BRC designed the experiments and MCR carried them out with support from NH, CS, and XL. JH
825 provided support on experimental setup and instrumentation. MCR prepared the manuscript with contributions from
826 all co-authors.

827 **Competing interests**

828 MCR is Lead Oceanographer and Head of MRV at Ebb Carbon, Inc. MDE is Co-Founder and Chief Scientific
829 Advisor at Ebb Carbon, Inc.

830 **Acknowledgements**

831 We would like to thank Stephen Abrams and Thomas Wilson at Stony Brook University Flax Pond Marine Lab for
832 technical assistance in experiment setup. We thank Chris Ikeda and Susan Curless of NOAA PMEL for support in
833 discrete sample analysis. We thank Mike Tyka for productive discussions. We thank Eyal Wurgaft for assistance in
834 TA titrations.

835 **Funding**

836 We acknowledge funding from The Grantham Foundation for the Protection of the Environment under the SEA
837 MATE (Safe Elevation of Alkalinity for the Mitigation of Acidification Through Electrochemistry) grant. In
838 addition, this research used the [XRD](#) facility of the Center for Functional Nanomaterials (CFN), which is a U.S.
839 Department of Energy Office of Science User Facility, at Brookhaven National Laboratory under Contract No. DE-
840 SC0012704. BRC and JH were funded through the Cooperative Institute for Climate, Ocean, and Ecosystem
841 Studies (CICOES) under NOAA Cooperative Agreement NA20OAR4320271 and supported by NOAA's PMEL.

842 **References**

843

844 Albright, R., Caldeira, L., Hoffelt, J., Kwiatkowski, L., Maclaren, J.K., Mason, B.M., Nebuchina, Y. et al.: Reversal
845 of ocean acidification enhances net coral reef calcification. *Nature*, 531, no. 7594: 362-365, 2016.

846 [Bach, L.T.: The additionality problem of ocean alkalinity enhancement. *Biogeosciences Discussion*. \[preprint\], in
847 *review*, 2023](#)

848 Bach, L. T., Gill, S.J., Rickaby, R.E.M., Gore, S., and Renforth, P.: CO₂ removal with enhanced weathering and
849 ocean alkalinity enhancement: potential risks and co-benefits for marine pelagic ecosystems. *Frontiers in
850 Climate*, 1, 7, 2019.

851 [Bainbridge, Z., Lewis, S., Bartley, R., Fabricius, K., Collier, C., Waterhouse, J., Garzon-Garcia, A., Robson, B.,
852 Burton, J., Wenger, A., and Brodie, J: Fine sediment and particulate organic matter: A review and case study on
853 ridge-to-reef transport, transformations, fates, and impacts on marine ecosystems. *Marine Pollution Bulletin*
854 *135*, pp. 1205-1220. 2018](#)

855 Berner, R. A., Lasaga, A.C., and Garrels, R.M.: Carbonate-silicate geochemical cycle and its effect on atmospheric
856 carbon dioxide over the past 100 million years. *Am. J. Sci.*(United States) 283, no. 7, 1983.

857 Boettcher, M., Chai, F. Cullen, J., Goeschl, T., Lampitt, R., Lenton, A., Oeschies, A. et al.: High level review of a
858 wide range of proposed marine geoengineering techniques. GESAMP Working Group Reports and Studies, 41,
859 2019.

860 [Broderson, K.E., Hammer, K.J., Schrammeyer, V., Floytrup, A., Rasheed, M.A., Ralph, P.J., Köhl, M., and Pederson,
861 O.: Sediment resuspension and deposition on seagrass leaves impedes internal plant aeration and promotes
862 phytotoxic H₂S intrusion. *Frontiers in Plant Science* 8. 2017](#)

863 [Burt, D.J., Fröb, F., & Ilyina, T.: The sensitivity of the marine carbonate system to regional ocean alkalinity
864 enhancement. *Frontiers in Climate* 3, 624075. 2021](#)

865 [Bustos-Serrano, H., Morse, J.W., & Millero, F.J.: The formation of whittings on the Little Bahama Bank. *Marine
866 Chemistry* 113, no. 1-2, pp. 1-8. 2009](#)

867 [Butenschön, M., Lovato, T., Masina, S., Caserini, S., and Grosso, M.: Alkalinization scenarios in the Mediterranean
868 Sea for efficient removal of atmospheric CO₂ and the mitigation of ocean acidification. *Frontiers in Climate* 3,
869 614537. 2021](#)

870 Carter, B. R., J. A. Radich, H. L. Doyle, and A. G. Dickson.: An automated system for spectrophotometric seawater
871 pH measurements. *Limnology and Oceanography: Methods*, 11, no. 1: 16-27, 2013.

872 Caserini, S., Storni, N., & Grosso, M.: The availability of limestone and other raw materials for ocean alkalinity
873 enhancement. *Global Biogeochemical Cycles*, 36, e2021GB007246. <https://doi.org/10.1029/2021GB007246>,
874 2022.

875 [Cross, J.N., Sweeney, C., Jewett, E.B., Feely, R.A., McElhany, P., Carter, B., Stein, T., Kitch, G.D., and Gledhill,
876 D.: Strategy for NOAA carbon dioxide removal research: A white paper documenting a potential NOAA CDR
877 science strategy as an element of NOAA's Climate Interventions Portfolio. NOAA Special Report. NOAA,
878 Washington, DC. DOI: 10.25923/gzke-8730. 2023](#)

879 Cyronak, T., Albright, R., and Bach, L.: Chapter 4.5: Field Experiments, *State Planet Discuss*. [preprint],
880 <https://doi.org/10.5194/sp-2023-9>, in review, 2023.

881 de Lannoy, C.-F., Eisaman, M.D., Jose, A., Karnitz, S.D., DeVaul, R.W., Hannun, K., and Rivest, J.L.B.: Indirect
882 ocean capture of atmospheric CO₂: Part I. Prototype of a negative emissions technology. *International journal of
883 greenhouse gas control*, 70: 243-253, 2018.

884 Dickson, A. G.: An exact definition of total alkalinity and a procedure for the estimation of alkalinity and total
885 inorganic carbon from titration data. *Deep Sea Research Part A. Oceanographic Research Papers*, 28(6), 609–
886 623, 1981.

887 Dickson, A. G.: The development of the alkalinity concept in marine chemistry. *Marine Chemistry*, 40(1–2), 49–63,
888 1992.

889 Dickson, A.G.: Thermodynamics of the dissociation of boric acid in synthetic seawater from 273.15 to 318.15 K.
890 *Deep Sea Research Part A. Oceanographic Research Papers*, 37, no. 5: 755-766, 1990.

891 Dickson, A.G., Sabine, C.L., and Christian, J.R.: Guide to best practices for ocean CO₂ measurements. North Pacific
892 Marine Science Organization, 2007.

893 [Eisaman, M. D., Parajuly, K., Tuganov, A., Eldershaw, C., Chang, N., Littau, K. A. CO₂ Extraction from Seawater
894 Using Bipolar Membrane Electrodialysis, *Energy Environ. Sci.*, 5: 7346. <https://doi.org/10.1039/e2ee03393e>, 2012.-](#)

895 Eisaman, M. D.; Rivest, J. L. B.; Karnitz, S. D.; De Lannoy, C.-F.; Jose, A.; DeVaul, R. W.; Hannun, K. Indirect
896 Ocean Capture of Atmospheric CO₂: Part II. Understanding the Cost of Negative Emissions. *International
897 Journal of Greenhouse Gas Control*, 70: 254–261, <https://doi.org/10.1016/j.ijggc.2018.02.020>, 2018.

898 Eisaman, M. D., Geilert, S., Renforth, P., Bastianini, L., Campbell, J., Dale, A. W., Foteinis, S., Grasse, P., Hawrot,
899 O., Löscher, C. R., Rau, G. H., and Rønning, J.: Assessing the technical aspects of ocean-alkalinity-

900 enhancement approaches, in: Guide to Best Practices in Ocean Alkalinity Enhancement Research, edited by:
901 Oschlies, A., Stevenson, A., Bach, L. T., Fennel, K., Rickaby, R. E. M., Satterfield, T., Webb, R., and Gattuso,
902 J.-P., Copernicus Publications, State Planet, 2-oae2023, 3, <https://doi.org/10.5194/sp-2-oae2023-3-2023>, 2023.

903 [Eisaman, M. D.: Pathways for marine carbon dioxide removal using electrochemical acid-base generation, *Front.*](#)
904 [Clim., 6, <https://doi.org/10.3389/fclim.2024.1349604>, 2024.](#)

905 Feely, R.A., Alin, S., Carter, B., Bednaršek, N., Hales, B., Chan, F., Hill, T.M., Gaylord, B., Sanford, E., Byrne,
906 R.H., Sabine, C.L., Greeley, D., Juranek, L., Chemical and biological impacts of ocean acidification along the
907 west coast of North America, *Estuarine, Coastal and Shelf Science*, doi: 10.1016/j.ecss.2016.08.043, 2016.

908 Feng, E. Y., Koeve, W., Keller, D.P., and Oschlies, A.: Model-Based Assessment of the CO₂ Sequestration Potential
909 of Coastal Ocean Alkalinization. *Earth's Future*, 5, no. 12: 1252-1266, 2017.

910 Fennel, K., Long, M. C., Algar, C., Carter, B., Keller, D., Laurent, A., Mattern, J. P., Musgrave, R., Oschlies, A.,
911 Ostiguy, J., Palter, J., and Whitt, D. B.: Modeling considerations for research on Ocean Alkalinity Enhancement
912 (OAE), *State Planet Discuss.* [preprint], <https://doi.org/10.5194/sp-2023-10>, in review, 2023.

913 Ferderer, A., Chase, Z., Kennedy, F., Schulz, K.G., and Bach, L.T.: Assessing the influence of ocean alkalinity
914 enhancement on a coastal phytoplankton community. *Biogeosciences* 19, no. 23: 5375-5399, 2022.

915 Friis, K.; Körtzinger, A.; Wallace, D. W. R. The Salinity Normalization of Marine Inorganic Carbon Chemistry
916 Data. *Geophys. Res. Lett.*, 30 (2). <https://doi.org/10.1029/2002GL015898>, 2003.

917 [Groen, A., Kittu, L., Ortiz Cortes, J., Schulz, K., and Riebesell, U.: Assessing the response of particulate organic](#)
918 [matter stoichiometry to ocean alkalisation. *Ocean Visions Summit, Atlanta, Georgia, USA,*](#)
919 [2023ocvi.conf27171G. 4-6 April 2023](#)

920 Hartmann, J., Suitner, N., Lim, C., Schneider, J., Marín-Samper, L., Arístegui, J., Renforth, P., Taucher, J., and
921 Riebesell, U.: Stability of alkalinity in ocean alkalinity enhancement (OAE) approaches—consequences for
922 durability of CO₂ storage. *Biogeosciences* 20, no. 4: 781-802, 2023.

923 Harvey, L.: Mitigating the atmospheric CO₂ increase and ocean acidification by adding limestone powder to
924 upwelling regions, *Journal of 640 Geophysical Research: Oceans*, 113, 2008.

925 He, J. and Tyka, M. D.: Limits and CO₂ equilibration of near-coast alkalinity enhancement, *Biogeosciences*, 20, 27–
926 43, <https://doi.org/10.5194/bg-20-27-2023>, 2023.

927 Ho, D. T., Bopp, L., Palter, J. B., Long, M. C., Boyd, P., Neukermans, G., and Bach, L.: Chapter 6: Monitoring,
928 Reporting, and Verification for Ocean Alkalinity Enhancement, *State Planet Discuss.* [preprint],
929 <https://doi.org/10.5194/sp-2023-2>, in review, 2023.

930 Ilyina, T., Wolf-Gladrow, D., Munhoven, G., and Heinze, C.: Assessing the potential of calcium-based artificial
931 ocean alkalization to mitigate rising atmospheric CO₂ and ocean acidification, *Geophysical Research Letters*,
932 40, 5909-5914, 2013.

933 IPCC: Summary for Policymakers. In: *Climate Change 2021: The Physical Science Basis, Contribution of Working*
934 *Group I to the Sixth Assessment Report of the Intergovernmental Panel on Climate Change*, edited by: Masson-
935 Delmotte, V., Zhai, P., Pirani, A., Connors, S. L., Péan, C., Berger, S., Caud, N., Chen, Y., Goldfarb, L., Gomis,
936 M. I., Huang, M., Leitzell, K., Lonnoy, E., Matthews, J. B. R., Maycock, T. K., Waterfield, T., Yelekçi, O., Yu,
937 R., and Zhou, B.: Cambridge University Press, Cambridge, United Kingdom and New York, NY, USA, 3–32,
938 <https://doi.org/10.1017/9781009157896.001>, 2022.

939 Isson, T. T., Planavsky, N. J., Coogan, L. A., Stewart, E. M., Ague, J. J., Bolton, E. W., et al.: Evolution of the
940 global carbon cycle and climate regulation on earth. *Global Biogeochemical Cycles*, 34, e2018GB006061.
941 <https://doi.org/10.1029/2018GB006061>, 2020.

942 [Johnson, K.M., King, A.E., and Sieburth, J.M.: Coulometric TCO₂ analyses for marine studies: An introduction.](#)
943 [Marine Chemistry 16, pp. 61-82. 1985.](#)

944 Jones, D.C., Ito, T., Takano, Y., and C.-W Hsu, C.-W.: Spatial and seasonal variability of the air-sea equilibration
945 timescale of carbon dioxide. *Global Biogeochemical Cycles*, 28(11), 1163–1178,
946 <https://doi.org/10.1002/2014GB004813>, 2014.

947 Kheshgi, H. S.: Sequestering atmospheric carbon dioxide by increasing ocean alkalinity, *Energy*, 20, 915-922, 1995.

948 Köhler, P., Hartmann, J., and Wolf-Gladrow, D.A.: Geoengineering potential of artificially enhanced silicate
949 weathering of olivine. *Proceedings of the National Academy of Sciences* 107, no. 47: 20228-20233, 2010.

950 La Plante, E., Chen, X., Bustillos, S., Bouissonnie, A., Traynor, T., Jassby, D., Corsini, L., Simonetti, D., and Sant,
951 G.: Electrolytic seawater mineralization and the mass balances that demonstrate carbon dioxide removal. *ACS*
952 *EST Engg.* <https://doi.org/10.1021/acsestengg.3c00004>, 2023.

953 Lee, K., Kim, T.-W., Byrne, R.H., Millero, F.J., Feely, R.A., and Liu, Y.-M.: The universal ratio of boron to
954 chlorinity for the North Pacific and North Atlantic oceans. *Geochimica et Cosmochimica Acta* 74, no. 6: 1801-
955 1811, 2010.

956 Lewis, E., Wallace, D., & Allison, L. J.: Program developed for CO₂ system calculations.
957 <https://doi.org/10.2172/639712>, 1998.

958 [Liu, X., Wang, Z.A., Byrne, R.H., Kaltenbacher, E.A., and Bernstein, R.E.: Spectrophotometric measurements of](#)
959 [pH in-situ: laboratory and field evaluations of instrumental performance. *Environmental Science & Technology*](#)
960 [40, no. 16, 5026-5044, 2006](#)

961 Lu, X., Ringham, M., Hirtle, N., Hillis, K., Shaw, C., Herndon, J., Carter, B.R., and Eisaman, M.D.:
962 Characterization of an Electrochemical Approach to Ocean Alkalinity Enhancement. In AGU Fall Meeting
963 Abstracts, vol. 2022, pp. GC31C-01. 2022.

964 Lueker, T.J., Dickson, A.G., and Keeling, C.D.: Ocean pCO₂ calculated from dissolved inorganic carbon, alkalinity,
965 and equations for K₁ and K₂: validation based on laboratory measurements of CO₂ in gas and seawater at
966 equilibrium. *Marine chemistry* 70, no. 1-3: 105-119, 2000.

967 Minx, J.C., Lamb, W.F., Callaghan, M.W., Fuss, S., Hilaire, J., Creutzig, F., Amann, T., et al.: Negative
968 emissions—Part 1: Research landscape and synthesis. *Environmental Research Letters* 13, no. 6: 063001, 2018.

969 Montserrat, F., Renforth, P., Hartmann, J., Leermakers, M., Knops, P., and Meysman, F.J.R.: Olivine dissolution in
970 seawater: implications for CO₂ sequestration through enhanced weathering in coastal environments.
971 *Environmental Science & Technology* 51, no. 7: 3960-3972, 2017.

972 Moras, C.A., Bach, L.T., Cyronak, T., Joannes-Boyau, R., and Schulz, K.G.: Ocean alkalinity enhancement—
973 avoiding runaway CaCO₃ precipitation during quick and hydrated lime dissolution. *Biogeosciences* 19, no. 15:
974 3537-3557, 2022.

975 National Academies of Sciences, Engineering, and Medicine. A research strategy for ocean-based carbon dioxide
976 removal and sequestration. 2021.

977 National Academies of Sciences, Engineering, and Medicine. Negative Emissions Technologies and Reliable
978 Sequestration: A Research Agenda. 2018.

979 Nduagu, E. "Production of Mg(OH)₂ from Mg-silicate rock for CO₂ mineral sequestration. Dissertation for Abo
980 Akademi University, 2012.

981 Oschlies, A., Bach, L., Rickaby, R., Satterfield, T., Webb, R. M., and Gattuso, J.-P.: Climate targets, carbon dioxide
982 removal and the potential role of Ocean Alkalinity Enhancement, *State Planet Discuss.* [preprint],
983 <https://doi.org/10.5194/sp-2023-13>, in review, 2023.

984 Pierrot, D., Lewis, E., and Wallace, D.W.R.: MS Excel program developed for CO₂ system calculations.
985 ORNL/CDIAC-105a. Carbon Dioxide Information Analysis Center, Oak Ridge National Laboratory, U.S.
986 Department of Energy, Oak Ridge, Tennessee, 2006.

987 Rau, G.H.: Electrochemical splitting of calcium carbonate to increase solution alkalinity: Implications for mitigation
988 of carbon dioxide and ocean acidity. *Environmental science & technology* 42, no. 23: 8935-8940, 2008.

989 Renforth, P., and Henderson, G.: Assessing ocean alkalinity for carbon sequestration. *Reviews of Geophysics* 55,
990 no. 3: 636-674, 2017.

991 Rigopoulos, I., Harrison, A.L., Delimitis, A., Ioannou, I., Efstathiou, A.M., Kyratsi, T., and Oelkers, E.H. : Carbon
992 sequestration via enhanced weathering of peridotites and basalts in seawater. *Applied Geochemistry* 91: 197-
993 207, 2018.

994 Rueda, O., Mogollón, J.M., Tukker, A., and Scherer, L.: Negative-emissions technology portfolios to meet the 1.5°
995 C target. *Global Environmental Change* 67: 102238, 2021.

996 Rogelj, J., Popp, A., Calvin, K. V., Luderer, G., Emmerling, J., Gernaat, D., Fujimori, S., Strefler, J., Hasegawa, T.,
997 Marangoni, G., Krey, V., Kriegler, E., Riahi, K., van Vuuren, D. P., Doelman, J., Drouet, L., Edmonds, J.,
998 Fricko, O., Harmsen, M., Havlík, P., Humpenöder, F., Stehfest, E., and Tavoni, M.: Scenarios towards limiting
999 global mean temperature increase below 1.5 °C, *Nat. Clim. Change*, 8, 325–332, [https://doi.org/10.1038/s41558-](https://doi.org/10.1038/s41558-018-0091-3)
1000 [018-0091-3](https://doi.org/10.1038/s41558-018-0091-3), 2018.

1001 Schulz, K. G., Bach, L. T., and Dickson, A. G.: Seawater carbonate system considerations for ocean alkalinity
1002 enhancement research, *State Planet Discuss.* [preprint], <https://doi.org/10.5194/sp-2023-12>, in review, 2023.

1003 Shaw, C., Ringham, M.C., Lu, X., Carter, B.R., Eisaman, M.D., and Tyka, M.: Understanding the Kinetics of
1004 Electrochemically derived Magnesium Hydroxide for Ocean Alkalinity Enhancement. In AGU Fall Meeting
1005 Abstracts, vol. 2022, pp. GC32I-0713. 2022.

1006 Song, S., Wang, Z.A., Gonnee, M.E., Kroeger, K.D., Chu, S.N., Li, D., and Liang, H.: An important
1007 biogeochemical link between organic and inorganic carbon cycling: Effects of organic alkalinity on carbonate
1008 chemistry in coastal waters influenced by intertidal salt marshes. *Geochimica et Cosmochimica Acta* 275:123-
1009 139, 2020.

1010 [Sutner, N., Faucher, G., Lim, C., Schneider, J., Moras, C.A., Riebesell, U., and Hartmann, J.: Ocean alkalinity](#)
1011 [enhancement approaches and the predictability of runaway precipitation processes- Results of an](#)

1012 [experimental study to determine critical alkalinity ranges for safe and sustainable application scenarios.](#)
1013 [EGUsphere \[preprint\], <https://doi.org/10.5194/egusphere-20223-2611>, 2023](#)
1014 Tyka, M.D., Arsdale, C.V., and Platt, J.C.: CO₂ capture by pumping surface acidity to the deep ocean. *Energy &*
1015 *Environmental Science* 15, no. 2: 786-798, 2022.
1016 Van Heuven, S., Pierrot, D., Rae, J., Lewis, E., & Wallace, D.: MATLAB program developed for CO₂ system
1017 calculations. ORNL/CDIAC-105b, 530, 2011.
1018 Vitillo, J. G., Eisaman, M.D., Aradóttir, E.S.P., Passarini, F., Wang, T., and Sheehan, S.W.: The role of carbon
1019 capture, utilization and storage for economic pathways that limit global warming to below 1.5° C." *Iscience*:
1020 104237, 2022.
1021 Wang, H., Pilcher, D. J., Kearney, K. A., Cross, J. N., Shugart, O. M., Eisaman, M. D., & Carter, B. R.: Simulated
1022 impact of ocean alkalinity enhancement on atmospheric CO₂ removal in the Bering Sea. *Earth's Future*, 11(1),
1023 e2022EF002816, 2023
1024 Wang, Z. A. and Cai, W. J.: Carbon dioxide degassing and inorganic carbon export from a marsh-dominated estuary
1025 (the Duplin River): A marsh CO₂ pump. *Limnol. Oceanogr.* 49, 341–354, 2004.
1026 Wolf-Gladrow, D. A., Zeebe, R. E., Klaas, C., Körtzinger, A., & Dickson, A. G.: Total alkalinity: The explicit
1027 conservative expression and its application to biogeochemical processes. *Marine Chemistry*, 106(1–2), 287–
1028 300, 2007.
1029 [Wurgaft, E., Steiner, Z., Luz, B., and Lazar, B.: Evidence for inorganic precipitation of CaCO₃ on suspended solids](#)
1030 [in the open water of the Red Sea, *Marine Chemistry*, 186, pp. 145–155, 2016.](#)
1031 [Wurgaft, E., Wang, Z., Churchill, J., Dellapenna, T., Song, S., Du, J., Ringham, M., Rivlin, T., and Lazar, B.:](#)
1032 [Particle triggered reactions as an important mechanism of alkalinity and inorganic carbon removal in river](#)
1033 [plumes, *Geophysical Research Letters*, 48, e2021GL093178, <https://doi.org/10.1029/2021GL093178>, 2021](#)
1034 [Zeebe, R.E., and Wolf-Gladrow, D.: CO₂ in seawater: equilibrium, kinetics, isotopes. Vol. 65, Gulf Professional](#)
1035 [Publishing, 2001.](#)
1036 [Zhang, H., and Byrne, R.H.: Spectrophotometric pH measurements of surface seawater at in-situ conditions:](#)
1037 [absorbance and protonation behavior of thymol blue. *Marine Chemistry* 52, no. 1, pp. 17-25. 1996](#)